Electronic and vibrational properties of $TiSe_2$ in the charge-density-wave phase from first principles

Raffaello Bianco,* Matteo Calandra, and Francesco Mauri
CNRS, UMR 7590, F-75005 Paris, France
and Sorbonne Universités, UPMC Univ Paris 06, IMPMC - Institut de Minéralogie, de Physique des Matériaux, et de Cosmochimie, 4 place Jussieu, F-75005 Paris, France
(Received 9 March 2015; revised manuscript received 7 June 2015; published 21 September 2015)

We study the charge-density-wave phase in $TiSe_2$ by using first-principles density functional theory calculations with the harmonic approximation for the electron-phonon coupling. We consider several local functionals and both experimental and theoretical cell parameters. The results obtained are very sensitive to the cell parameters used. However, we show that, if the experimental cell is used, harmonic calculations are able to reproduce not only the structural instability of $TiSe_2$ but also the effective distortion observed in the experiments, irrespective of the local functional used. If the experimental cell is used, the energy profile obtained by displacing the atoms is independent of the local functional considered too. With the semiempirical functional Grimme B97-D, aimed at describing better the van der Waals forces coupling the $TiSe_2$ layers, the theoretical cell is in agreement with the experimental one and the structural analysis gives results analogous to the ones obtained with the experimental cell. We also present a study of the electronic structure evolution under the charge-density-wave deformation. In particular, we apply the unfolding technique in order to compare the calculated energy bands for the distorted structure with angle-resolved photoemission spectroscopy (ARPES) data taken at low temperature. In order to obtain a better agreement between ARPES and the calculated bands, both at high and low temperature, we investigate the effect of the correlation on the electrons of the localized Ti-3*d* orbitals by using the LDA + *U* method. We show that within this approximation the electronic bands for both the undistorted and distorted structure are in good agreement with ARPES. On the other hand, *U* eliminates the phonon instability of the system. A possible explanation for this counterintuitive result is proposed. Particularly, the possibility of taking into account the dependence of the parameter *U* on the atomic positions is suggested.

DOI: 10.1103/PhysRevB.92.094107 PACS number(s): 71.15.Mb, 71.20.Be, 63.20.kd

I. INTRODUCTION

The group IV*b* transition metal diselenide 1T-$TiSe_2$ (space group $P\bar{3}m1$) is a layered compound which has received considerable attention because of its interesting physical properties. In particular, below the critical temperature $T_{CDW} \simeq$ 200 K, it undergoes a commensurate charge density wave (CDW) transition, with the formation of a $2\times2\times2$ superlattice structure (space group $P\bar{3}c1$) accompanied by the softening of a zone boundary phonon and changes in the transport properties [1–3]. In spite of many experimental and theoretical studies, the driving force of this structural phase transition remains controversial. Several mechanisms have been proposed for the origin of the instability in $TiSe_2$ and they can be roughly classified into two main groups depending on the driving role played either by the electrons or by the lattice. In fact, a charge density wave occurs always simultaneously with a periodic lattice distortions, so with both a modification of the electron and phonon spectra, but it is still unclear if what is observed is primarily an instability of the electronic system or of the lattice [4,5]. The excitonic insulator model belongs to the first case [6–8], where the CDW is essentially viewed as a many-body effect originated by the poorly screened electron-hole Coulomb interaction giving rise to a condensate of excitons and a consequent distortion. In the second family, we find Peierls and Jahn-Teller band-type mechanisms [9,10], where the instability essentially comes from the electron-phonon coupling leading to a lattice distortion that lowers the total energy of the system. Quite recently, a scenario where the CDW transition is driven by a combination of excitonic ordering and Jahn-Teller effect has also been proposed [11,12]. The CDW phase competes with superconductivity since $TiSe_2$ is not superconducting at low temperatures but the CDW is suppressed and the superconductivity is stabilized either by Cu intercalation [13] or pressure [14]. For this reason, a deep and definitive understanding of the CDW occurrence would be interesting both for conceptual reasons and technological applications.

There is ample theoretical literature on the distorted phase of $TiSe_2$. The results obtained by Motizuki and coworkers [3,15–17], who developed a general microscopic theory of the structural instability in dichalcogenides, through the band-type Jahn-Teller mechanism by using the tight-binding approximation, are very important. In particular, they studied the instability and the electronic structure of the CDW phase in $TiSe_2$ by using a tight-binding model with the free parameters set by fitting the energy bands with the results of the self-consistent local density calculation made for the undistorted structure in Ref. [18].

In this paper, we present the results of first-principles density functional theory (DFT) calculations of the CDW instability in $TiSe_2$ with the harmonic approximation for the electron-phonon coupling. Our aim is to investigate at what level an unbiased first-principles calculation is able to recover the experimental results and to analyze the specific role of the electron-phonon coupling in the appearance of the CDW. The calculations have been performed with several local functionals and experimental or theoretical unit cells. The results obtained depend on the cell parameters used. We show that, if the experimental unit cell is used, through DFT it is possible to observe a structural instability at the *L* and *M*

*raffaello.bianco@impmc.upmc.fr

points of the Brillouin zone (BZ) consistent with a $2\times2\times2$ (L) and $2\times2\times1$ (M) real-space superstructure [19], regardless of the local functional used. We present an analysis of both the M and L distortion patterns and we show that the distortion giving the most stable structure is the so-called triple-point pattern in L, the same kind of distortion observed in the experiments (and described the first time by di Salvo and coworkers in Ref. [1]). Moreover, the magnitude of the lattice distortion calculated is close to the experimental one. If the experimental cell parameters are used, these results are independent of the local functional.

The theoretical cell parameters are obtained by relaxing the cell in order to achieve zero theoretical pressure. The values of the theoretical lattice parameters strongly depend on the functional used and, in general, for standard local functionals, they are not in good agreement with the experimental ones. However, as adjacent layers in $TiSe_2$ are coupled by van der Waals forces, we considered also the Grimme B97-D semiempirical functional, which is aimed at describing more accurately this kind of interaction [20]. We show that with that functional the theoretical cell parameters are in good agreement with the experiment and so, as expected, in this case the structural analysis with the theoretical cell gives results analogous to the ones obtained with the experimental cell.

After the structural analysis, we present the results of the calculations for the electronic structure of the system. In DFT pseudopotential calculations the system in the undistorted phase appears to be metallic, with the Fermi surface depending on the unit cell used. We show the effect of the distortion on the energy dispersion around the Fermi level and in particular on the density of states (with results at some level compatible with other results present in literature [16]). Moreover, we compare the calculated electronic bands for the undistorted and distorted phase with data taken from an ARPES experiment at high and low temperature, respectively. Particularly, for the distorted phase, we unfold the bands into the undistorted BZ in order to make the comparison more efficient.

In order to improve the match between the calculated bands and ARPES, we investigated the effect of the Coulomb repulsion on the electrons of the localized Ti-3d orbitals by using the LDA + U method. We show that U significantly improves the comparison with ARPES but it also spoils the lattice instability. We discuss how these somehow counterintuitive results could be interpreted.

The paper is organized as follows. In Sec. II, we summarize the method and the parameters used. Then, in Sec. III, we present the *ab initio* structural analysis of the $TiSe_2$ instability and CDW phase. Afterwards, in Sec. IV, we analyze the electronic structure of the undistorted and distorted phases, and in Sec. V, we compare the bands with ARPES data (in Sec. V A, for the LDA and Grimme B97-D functionals and in Sec. V B, for the LDA + U case). Finally, conclusions are presented in Sec. VI. In Appendix, we provide some details about the unfolding technique.

II. COMPUTATIONAL DETAILS

All calculations were performed within the framework of DFT using the QUANTUM ESPRESSO package [21] which uses a plane-wave basis set to describe the valence-electron wave functions and charge density. For the exchange-correlation functional (xc functional) we used both the Perdew-Zunger local density approximation (LDA) [22] and the Perdew-Burke-Ernzerhof conjugate gradient approximation (GGA) [23]. As adjacent layers in $TiSe_2$ are coupled by van der Waals forces, we also considered Grimme B97-D, a GGA-type semiempirical functional aimed at describing more accurately this kind of interaction [20]. In the text, we will indicate this functional also with GGA^{VdW}. The phonons have been calculated using density functional perturbation theory (DFPT) in the linear response [24].

We used a cutoff of 85 Ry and 850 Ry (1 Ry $\approx$ 13.6 eV) for the wave functions and the charge density, respectively; the BZ integration has been performed with a Monkhorst-Pack grid [25] of $24\times24\times12$ **k** and a Hermite-Gaussian smearing of 0.01 Ry. The self-consistent solution of the Kohn-Sham equations was obtained when the total energy changed by less than 10^{-10} Ry. We studied the system with internal theoretical coordinates (i.e., zero theoretical forces) and with both experimental and theoretical cell (i.e., zero theoretical pressure). The theoretical parameters have been obtained by relaxing the structure starting from the experimental parameters [26] until the forces on the atoms were less than 10^{-3} Ry a_0^{-1} ($a_0 \approx 0.529\,177$ Å is the Bohr radius) and the pressure less than 0.5 Kbar.

The values of the geometrical parameters obtained for different local functionals are reported in Table I. As it can be seen, the values of the theoretical lattice parameters are very sensitive to the local functional used. For example, the distance c between layers is underestimated in LDA and overestimated in GGA, in the second case, with quite an important relative error around 12% for c. As expected, the best agreement between theory and experiment is obtained by using the GGA^{VdW} functional.

In order to take into account the strong correlation effects due to the localized d orbitals of Ti, we also considered the LDA + U method in the simplified form described in Refs. [27,28]. Since we consider the Hubbard-like correction

TABLE I. Experimental and theoretical geometrical parameters of the system in the undistorted phase (cf. Fig. 1): hexagonal lattice constant a, distance c between the layers, distance h between the Se and the Ti planes in a layer and horizontal projection R of distance between Se and Ti in an octahedron. The subscripts "Exp" and "Th" refer to the experimental and theoretical cell, respectively. Notice that for the undistorted phase, R is fixed by the unit cell geometry (it must be equal to $a\sqrt{3}/3$ in order to obtain a null force along the planar direction), whereas this is not true anymore in the distorted phase (cf. Table VI).

	a (Å)	c (Å)	h (Å)	R (Å)
Exp	3.540	6.007	1.532	2.044
LDA_{Exp}	3.540	6.007	1.499	2.044
GGA_{Exp}	3.540	6.007	1.534	2.044
GGA^{VdW}_{Exp}	3.540	6.007	1.532	2.044
LDA_{Th}	3.434	5.792	1.535	1.982
GGA_{Th}	3.536	6.719	1.548	2.041
GGA^{VdW}_{Th}	3.510	6.165	1.553	2.026

for one orbital and no spin, there is a single additional parameter U in the calculation.

We essentially performed two kinds of analysis. On one hand, we calculated the variation of the phonon frequencies in L and M with the value of U for the experimental cell and theoretical internal coordinates obtained by relaxing the atomic positions for each value of U. In this case, the phonon frequencies have been obtained by using the finite difference method in Ref. [29] with a $2\times2\times2$ cell and atomic displacements of $1/66 \simeq 0.015$ Å. A mesh grid of $24\times24\times12$ **k** for the supercell Brillouin zone and a Hermite-Gaussian smearing of 0.125×10^{-2} Ry have been used for the related self-consistent calculations of the forces.

On the other hand, we calculated, by linear response, a first-principles estimate of U for the $\mathrm{LDA_{Exp}}$ case in the undistorted phase, through the difference between the screened and bare second derivative of the total energy with respect to the occupation of the Ti-3d orbital [27]. For an input value U_{in}, used to define the starting system, the linear-response calculation returns a different output value $U_{\mathrm{out}} \neq U_{\mathrm{in}}$ but, in order to be consistent and replace the LDA interaction term with the corresponding Hubbard correction, the ideal case in which $U_{\mathrm{in}} = U_{\mathrm{out}} \equiv U$ should be considered. In fact, even if it is a common practice to simply compute the *ab initio* value of U in one step with $U_{\mathrm{in}} = 0$, this consideration can be relevant, especially if the LDA and LDA + U systems are qualitatively different [30]. In our case, in particular, the effect of U is to open a gap between the bands with the result of obtaining, for $U \simeq 4$, a metal-insulator transition (see Sec. V B). For this reason, we determined U with a self-consistent procedure starting from the unperturbed system ($U_{\mathrm{in}} = 0$) and using, step by step, the obtained U_{out} as U_{in} for the subsequent calculation. For each step, we obtained the result first by performing the linear response calculation on a $2\times2\times2$ cell and then extrapolating the outcome to a $6\times6\times6$ cell (see Ref. [27] for details). With this procedure we converged in a few steps to the value $U \simeq 3.902$ eV. Since we decided to work with a fixed configuration, for all the steps we always used the same internal coordinates obtained by relaxing the atomic positions with $U = 0$; moreover, in order to achieve a precision of 10^{-3} eV for the converged value of U, we set the energy convergence threshold for self-consistency equal to 10^{-14} Ry.

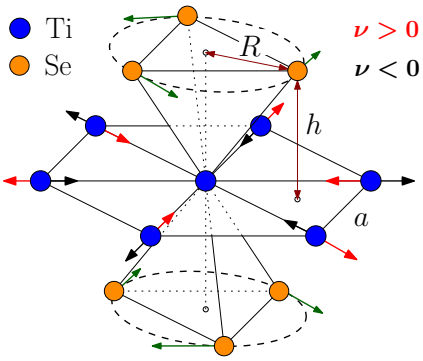

FIG. 1. (Color online) Octahedral structure of $TiSe_2$ in a layer. The Se atoms in the upper and lower plane are on circles of radius R at distance h from the Ti atoms plane. The value of the hexagonal lattice parameter a, the distance c between two layers (not shown) and h completely define the system (the value of R is fixed by the geometry in the undistorted phase). The rotational displacement of the Se atoms in a triple-$\boldsymbol{q}$ mode and the attraction (repulsion) exerted over the Ti atoms by two close Se's for $\nu > 0$ ($\nu < 0$) is also shown (see the main text for the definition of ν).

III. STRUCTURAL ANALYSIS OF THE CDW

In the BZ of $TiSe_2$, the three L points—L_1, L_2, L_3—and the three M points—M_1, M_2, M_3—are equivalent thanks to the three-fold rotation symmetry of the system (see Fig. 2). The vectors $\boldsymbol{q}_{L_i}$ and $\boldsymbol{q}_{M_i}$ from Γ to L_i and M_i, respectively, have reduced components (cf. Fig. 2):

$$\begin{aligned} \boldsymbol{q}_{M_1} &= \left(\tfrac{1}{2},0,0\right), \quad \boldsymbol{q}_{L_1} = \left(\tfrac{1}{2},0,\tfrac{1}{2}\right), \\ \boldsymbol{q}_{M_2} &= \left(0,-\tfrac{1}{2},0\right), \quad \boldsymbol{q}_{L_2} = \left(0,-\tfrac{1}{2},\tfrac{1}{2}\right), \\ \boldsymbol{q}_{M_3} &= \left(-\tfrac{1}{2},\tfrac{1}{2},0\right), \quad \boldsymbol{q}_{L_3} = \left(-\tfrac{1}{2},\tfrac{1}{2},\tfrac{1}{2}\right). \end{aligned} \tag{1}$$

In L_i and M_i, the small group is C_{2h} and the decomposition in irreducible representations is

$$2A_u \oplus 2A_g \oplus 4B_u \oplus B_g. \tag{2}$$

By using the density functional perturbation theory (DFPT), we computed the phonon frequencies at M and L. We found that in all the cases the lowest phonon mode has symmetry A_u with frequency always imaginary except in the $\mathrm{LDA_{Th}}$ case. The values for the phonon frequencies in the $\mathrm{GGA_{Th}^{VdW}}$ case are shown in Table II and the frequencies of the lowest mode for all the cases are reported in Table III. When a phonon

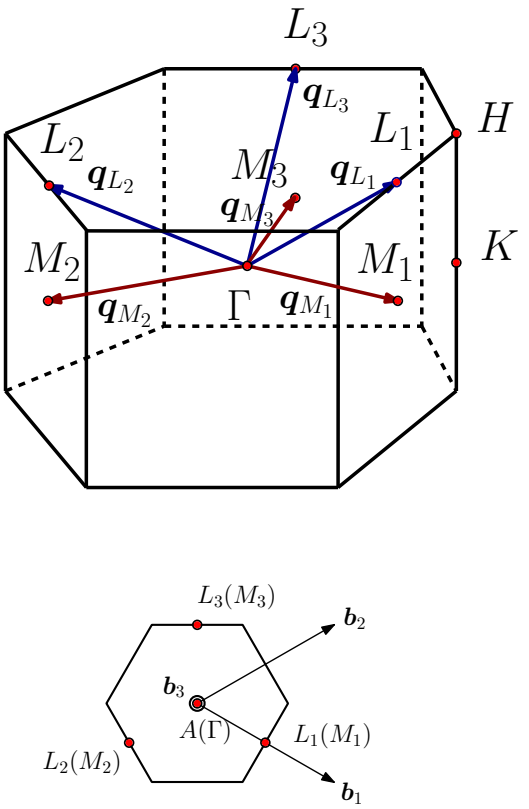

FIG. 2. (Color online) Brillouin zone of $TiSe_2$. The bottom figure is the BZ as seen from above. The $\boldsymbol{b}_i$ are the reciprocal lattice basis vectors ($\boldsymbol{b}_3$ is orthogonal to the layers).

TABLE II. Phonon frequencies with relative mode symmetries at L and M in the $\mathrm{GGA}^{\mathrm{VdW}}_{\mathrm{Th}}$ case.

	ω_L (meV)	ω_M (meV)
A_u	−10.00	−9.33
B_u	12.18	12.69
A_u	14.27	14.62
B_g	17.37	17.25
B_u	17.95	17.57
A_g	20.33	20.44
A_g	23.67	23.48
B_u	24.78	24.93
B_u	37.00	37.84

frequency ω is imaginary, we conventionally indicate it with the negative value $-|\omega|$.

A. *Ab initio* analysis of the structural instability

The imaginary phonon frequencies at M and L correspond to a structural instability consistent with a 2×2×1 (M) or a 2×2×2 (L) real-space superstructure. In order to study the 2×2×2 distortions, we consider the corresponding supercell of the undistorted crystal (which has 24 atoms) and the 72-dimensional space $\mathcal{V}$ whose general element $\boldsymbol{d} \equiv d_{i\alpha}$ is the displacement of the ith atom of the supercell along the Cartesian direction α.

For the 2×2×2 superstructure, the eight points Γ, A, L_i, and M_i of BZ refold to the Γ point. Therefore, the space $\mathcal{V}$ is equal to the orthogonal sum of the corresponding nine-dimensional subspaces $\mathcal{V}_\Gamma$, $\mathcal{V}_A$, $\mathcal{V}_{L_i}$, $\mathcal{V}_{M_i}$:

$$\mathcal{V}_L \equiv \bigoplus_{i=1}^{3} \mathcal{V}_{L_i}, \quad \mathcal{V}_M \equiv \bigoplus_{i=1}^{3} \mathcal{V}_{M_i}, \tag{3}$$

whose vectors describe distortions with a definite modulation character with respect to the original 1×1×1 unit cell of the undistorted phase. In particular, $\mathcal{V}_{L_i}$ and $\mathcal{V}_{M_i}$ are made of plane-wave lattice distortions with wave vector $\boldsymbol{q}_{L_i}$ and $\boldsymbol{q}_{M_i}$, respectively, that is, distortions having the atomic displacement of the kth atom in the lth unit cell given by

$$\boldsymbol{u}_{lk} = \boldsymbol{\epsilon}_k \cos(\boldsymbol{q} \cdot \boldsymbol{R}_l), \qquad \boldsymbol{q} \in \left\{\boldsymbol{q}_{L_i}, \boldsymbol{q}_{M_i}\right\}, \tag{4}$$

where $\boldsymbol{R}_l$ is the lth lattice vector and $\boldsymbol{\epsilon}_k$ gives the amplitude of the displacement for the kth atom in the unit cell of the origin.

If $E(\boldsymbol{d})$ is the energy of the system per supercell as a function of the 2×2×2 distortion, in the harmonic approximation it is

$$E(\boldsymbol{d}) \simeq E(0) + \frac{1}{2} \sum_{i\alpha j\beta} \left.\frac{\partial^2 E}{\partial d_{i\alpha} \partial d_{j\beta}}\right|_{\boldsymbol{d}=0} d_{i\alpha}\, d_{j\beta} \tag{5}$$

$$\equiv E(0) + \frac{1}{2} \sum_{i\alpha j\beta} C_{i\alpha, j\beta}\, d_{i\alpha}\, d_{j\beta}, \tag{6}$$

and, by grouping the two indices $(i\alpha) \equiv I$, we obtain a real-symmetric 72×72 matrix C_{IJ}, which has $N = 72$ couples of real eigenvalues and eigenvectors $(\lambda, \boldsymbol{d}^{(\lambda)})$. With the distortion $\boldsymbol{d}^{(\lambda)}$ the system has the variation of energy:

$$dE = \frac{\lambda}{2} \|\boldsymbol{d}^{(\lambda)}\|^2, \tag{7}$$

where $\|\boldsymbol{d}^{(\lambda)}\|$ is the euclidean norm of $\boldsymbol{d}^{(\lambda)}$. Thus, a negative eigenvalue corresponds to a displacement that lowers the energy of the system.

By using the DFPT, we calculated C_{IJ} and subsequently we diagonalized it. Because of the symmetry, we obtained the same spectrum for the three spaces $\mathcal{V}_{L_i}$ and the same spectrum for the three spaces $\mathcal{V}_{M_i}$, the corresponding displacements being related by threefold rotations. Consistently with the phonon analysis, we found, in each of these spaces, two eigenspaces with symmetry A_u, one of them with negative eigenvalue. Since we are interested in the instabilities of the system, we focus on this kind of distortions.

B. The A_u distortions

The displacements A_u, for a point L_i or M_i, are transversal to the direction of propagation $\boldsymbol{q}$, planar (i.e., no component outside the layer plane) and opposite for selenium atoms Se_1 and Se_2 on two adjacent wave fronts. We indicate with $-\nu$ the ratio between the displacements of the titanium atoms on a wave front and the selenium atoms Se_1 on an adjacent wave front:

$$A_u: \quad \begin{cases} \boldsymbol{\epsilon}_k \perp \boldsymbol{q}, \\ \boldsymbol{\epsilon}^z_k = 0, \\ \boldsymbol{\epsilon}_{\mathrm{Se}_2} = -\boldsymbol{\epsilon}_{\mathrm{Se}_1}, \\ \boldsymbol{\epsilon}_{\mathrm{Ti}} = -\nu\, \boldsymbol{\epsilon}_{\mathrm{Se}_1}, \end{cases} \tag{8}$$

z being the direction orthogonal to the layers. Thus, the sign of ν indicates if the displacement of two adjacent Ti and Se front waves are in phase ($\nu < 0$) or out of phase ($\nu > 0$) (see Fig. 3).

These modes form a two-dimensional vector space $2A_u$ made of displacements along a fixed line, where the only two free parameters left are the values of the shifts. We indicate with δTi the shift of the Ti atoms on a displacement wave front along a given direction and with δSe the displacement of the Se atoms on an adjacent wave front along the opposite direction (see Fig. 3). It is $\nu = \delta\mathrm{Ti}/\delta\mathrm{Se}$. By using the two parameters δTi and δSe, the space $2A_u$ can be represented as in Fig. 4. By symmetry, two displacements with opposite values for both δTi and δSe are equivalent, whereas by changing the relative phase between the shifts of the Se and the Ti atoms, we obtain two different configurations. In fact, a significant parameter is the ratio ν, which identifies a one-dimensional subspace $A_u(\nu)$ of $2A_u$. Therefore, a general $\boldsymbol{d} \in 2A_u$ is uniquely identified either by ν and $\|\boldsymbol{d}\|$ or, for example, by ν and δTi (δSe).

TABLE III. Phonon frequencies of the lowest mode (A_u) at L and M for the cases analyzed.

	ω_L (meV)	ω_M (meV)
$\mathrm{LDA}_{\mathrm{Exp}}$	−10.38	−9.17
$\mathrm{GGA}_{\mathrm{Exp}}$	−9.83	−8.28
$\mathrm{GGA}^{\mathrm{VdW}}_{\mathrm{Exp}}$	−9.61	−8.03
$\mathrm{LDA}_{\mathrm{Th}}$	+4.32	+7.13
$\mathrm{GGA}_{\mathrm{Th}}$	−13.14	−13.18
$\mathrm{GGA}^{\mathrm{VdW}}_{\mathrm{Th}}$	−10.01	−9.34

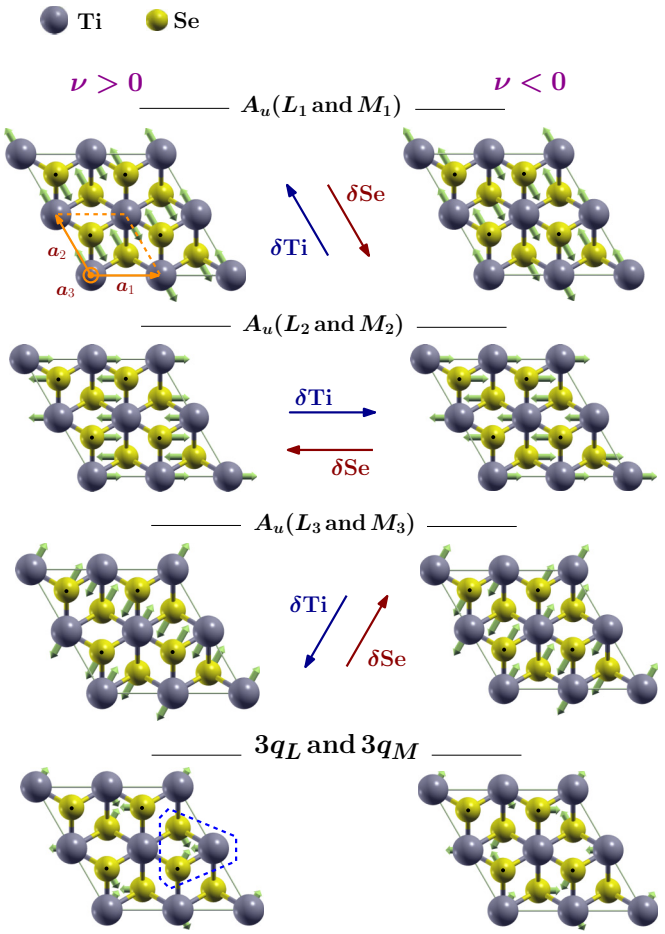

FIG. 3. (Color online) Schematic representation of the atomic displacements in the 2×2×2 cell of a single layer viewed from above for the three A_u modes in the points L_i and M_i and the triple modes $3\boldsymbol{q}_L$ and $3\boldsymbol{q}_M$. The two non-equivalent cases with $\nu > 0$ (left-hand figures) and $\nu < 0$ (right-hand figures) are shown, ν being the ratio between δTi and δSe. The Se atoms with a dot are on the upper plane with respect to the Ti atoms plane. In the first picture, the direct lattice basis $\boldsymbol{a}_i$ and the 1×1×1 unit cell are also drawn. The two central arrows indicate the positive directions used to measure the shifts δTi and δSe. In the $3\boldsymbol{q}$ mode with $\nu > 0$, a three atom cluster is highlighted with a dotted line. Notice that the triple-$\boldsymbol{q}$ modes shown are not equal to the sum of the A_u single-$\boldsymbol{q}$ modes represented as, otherwise, the displacements should be larger (the displacements of the atoms in a triple mode are two times larger than the displacements of the component single modes).

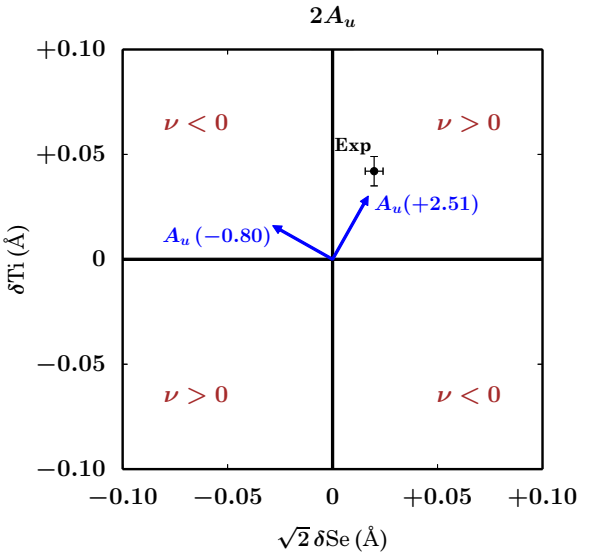

FIG. 4. (Color online) Diagram representing the distortion space $2A_u$ in L and M as a function of the displacements (δSe,δTi). The factor $\sqrt{2}$ on the horizontal axis comes from the two Se atoms in the unit cell and it is necessary in order to convert the orthogonality condition in $2A_u$ into the Euclidean orthogonality on the diagram. A line on this plot represents a one-dimensional subspace $A_u(\nu)$ with a specific ratio $\nu = \delta\text{Ti}/\delta\text{Se}$. As an example, the two orthogonal vectors corresponding to the A_u distortion modes of the $\text{GGA}^{\text{VdW}}_{\text{Th}}$ case are drawn. The point corresponding to the CDW distortion experimentally observed [1] is also drawn.

Each of the two orthogonal one-dimensional eigenspaces of symmetry A_u found by diagonalizing C_{IJ} is characterized by a specific value of the ratio, one positive and the other negative. In fact, it can be shown that two generic one-dimensional subspaces $A_u(\nu_1)$ and $A_u(\nu_2)$, corresponding to different values of the ratio $\nu = \nu_1$ and $\nu = \nu_2$, are orthogonal if and only if $\nu_1\nu_2 = -2$. We found that, in all the studied cases and in both points M and L, the A_u with the smallest eigenvalue λ corresponds always to the positive ratio $\nu > 0$, that is, to the out of phase distortion. For the studied cases, the values found for the smallest λ and the corresponding ν in the points L (λ_L, ν_L) and M (λ_M, ν_M) are reported in Table IV. From now on, we analyze only the cases where the system displays instability, therefore we do not consider LDA_{Th} anymore.

The value ν_L (ν_M) defines (up to a sign) three orthogonal unit vectors $\hat{\boldsymbol{d}}_{L_i}$ ($\hat{\boldsymbol{d}}_{M_i}$) corresponding to degenerate displacements of type A_u, which generate a three-dimensional space $\mathcal{V}_L^-$ ($\mathcal{V}_M^-$). By considering displacement vectors $\boldsymbol{d}$ in this space with an increasing modulus $\|\boldsymbol{d}\|$ but fixed direction, we can study the energy variation of the system along a pattern. We observe that the energy, after an initial parabolic decrease, starts departing from the harmonic regime, reaches a minimum and then increases (cf. Fig. 5). The minimum along this energy path corresponds to the configuration giving the most stable structure obtainable with that kind of distortion. In general, different patterns in $\mathcal{V}_L^-$ ($\mathcal{V}_M^-$) return different results as for finite displacements the symmetries of the lattice are not preserved.

C. The single-point and triple-point patterns

The displacement pattern of type A_u characterized by a unit vector $\hat{\boldsymbol{d}}_{L_i}$ ($\hat{\boldsymbol{d}}_{M_i}$) is also called a *single-$\boldsymbol{q}_L$ pattern* (*single-$\boldsymbol{q}_M$ pattern*). In Fig. 5, we show, for the several studied cases, the energy path for the single-$\boldsymbol{q}$ patterns in L and M. As we can see the distortion of type L returns always a structure more stable than the distortion of type M, except in the GGA_{Th} case where the two energy patterns approximatively coincide, meaning that the interaction between layers plays a non-negligible role in the minimization of the total energy unless their distance is large enough. Moreover, as long as the cell dimensions are comparable, we find similar results

TABLE IV. Values of the eigenvalue λ and of the ratio $\nu = \delta\mathrm{Ti}/\delta\mathrm{Se}$ for the A_u distortions in L and M corresponding to the smallest eigenvalue. Last row: value of the ratio measured for the CDW distortion [1].

	λ_M	ν_M	λ_L	ν_L
$\mathrm{LDA_{Exp}}$	−1.07	2.89	−1.37	2.93
$\mathrm{GGA_{Exp}}$	−0.89	2.60	−1.26	2.53
$\mathrm{GGA_{Exp}^{VdW}}$	−0.84	2.64	−1.20	2.56
$\mathrm{LDA_{Th}}$	+0.69	2.34	+0.25	2.42
$\mathrm{GGA_{Th}}$	−2.26	2.46	−2.25	2.43
$\mathrm{GGA_{Th}^{VdW}}$	−1.14	2.51	−1.31	2.46
$\nu_{\mathrm{CDW}}^{\mathrm{Exp}}$	–	–	–	3.42 ± 1.48

irrespective of the local functional used. Instead, in the $\mathrm{GGA_{Th}}$ case, where the distance between the layers is larger (see Table I), the energy gain due to the distortion is higher.[1] These considerations lead to the conclusion that the suppression of the instability in the $\mathrm{LDA_{Th}}$ case is due to the geometry of the unit cell, the LDA theoretical cell parameters being smaller than the experimental ones (see Table I).

The patterns characterized by the unit vectors $\hat{\boldsymbol{d}}_{3L}$ and $\hat{\boldsymbol{d}}_{3M}$ obtained by combining the three directions $\hat{\boldsymbol{d}}_{L_i}$ and $\hat{\boldsymbol{d}}_{M_i}$:

$$\hat{\boldsymbol{d}}_{3M} \equiv \sum_{i=1}^{3} \frac{1}{\sqrt{3}} \hat{\boldsymbol{d}}_{M_i}, \quad \hat{\boldsymbol{d}}_{3L} \equiv \sum_{i=1}^{3} \frac{1}{\sqrt{3}} \hat{\boldsymbol{d}}_{L_i}, \tag{9}$$

are called a *triple-*$\boldsymbol{q}_L$ ($3\boldsymbol{q}_L$) *pattern* and a *triple-*$\boldsymbol{q}_M$ ($3\boldsymbol{q}_M$) *pattern*, respectively. In fact, by definition, a general triple-$\boldsymbol{q}$ distortion of type L (M) is obtained by superimposing, with equal weights, three A_u distortions for the points L_i (M_i) having the same values of δTi and δSe.

In a layer, the shifts of the atoms in a $3\boldsymbol{q}$ distortion can be described by considering the $\mathrm{TiSe_6}$ octahedral structure of the system [31] (see Fig. 1). We distinguish two kinds of Ti and Se atoms: in one the Ti(α) atoms do not move and are in the middle of Ti(α)Se(α)$_6$ octahedra where the three Se(α) atoms above Ti(α) and the three Se(α) atoms below Ti(α) rotate with opposite direction. Therefore there are couples of Se(α)'s that become closer and, depending on whether the component three modes have $\nu > 0$ or $\nu < 0$, they attract or repulse a Ti(β) atom [in the first case, as a consequence, we observe a Ti(β)-Se(α) bond shortening and the formation of three-atom clusters Ti(β)Se(α)$_2$ in the system]. In the distortion we also have Se(β) atoms, which are not involved in any rotation [they are originally in octahedra centered around Ti(β) atoms] but stay in their position.

For an adjacent layer, depending on whether we are considering a $3\boldsymbol{q}_M$ or a $3\boldsymbol{q}_L$ distortion, the displacement of the atoms is the same or the opposite one [i.e., in the $3\boldsymbol{q}_L$ case if in one layer the Se(α)'s on the upper plane and lower plane show a clockwise and a counterclockwise rotation, respectively, the opposite happens in an adjacent layer]. Two $3\boldsymbol{q}$ distortions with $\nu > 0$ and $\nu < 0$, in a layer and view from above, are shown in Fig. 3.

[1]This corrects a statement in Ref. [46] about the irrelevance of c in the lattice instability.

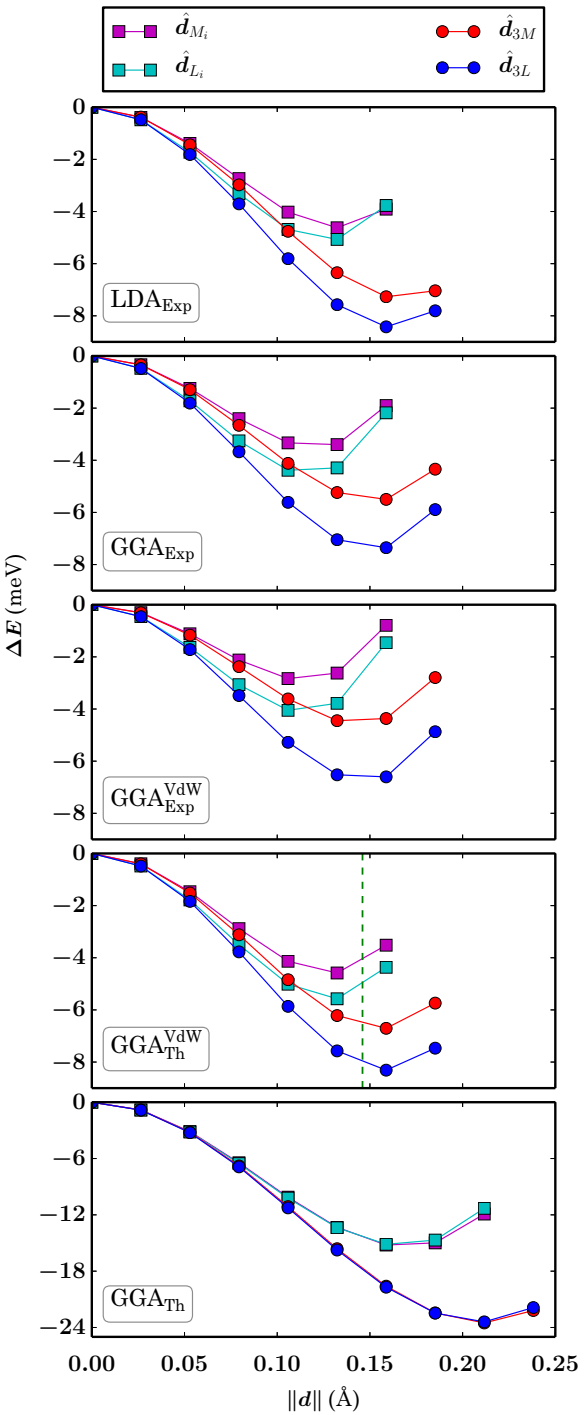

FIG. 5. (Color online) Variation of the energy with respect to the undistorted phase obtained by moving the atoms according to different patterns. The unit vectors $\hat{\boldsymbol{d}}_{L_i}$, $\hat{\boldsymbol{d}}_{M_i}$, $\hat{\boldsymbol{d}}_{3L}$, $\hat{\boldsymbol{d}}_{3M}$ characterize a single $\boldsymbol{q}_{L_i}$ and $\boldsymbol{q}_{M_i}$ mode, and a triple $\boldsymbol{q}_L$ and $\boldsymbol{q}_M$ mode, respectively. The vertical dashed line in the $\mathrm{GGA_{Th}^{VdW}}$ plot marks the point where the calculations of Fig. 7 have been performed.

D. The CDW distortion

In their seminal paper, Di Salvo and coworkers stated that according to neutron-diffraction measurements and symmetry considerations, the lattice distortion experimentally observed with the CDW is a $3\boldsymbol{q}_L$ mode with $\nu > 0$, with data taken at

77 K, which best fitted with the values [1]

$$\delta \mathrm{Ti}^{\mathrm{Exp}} = (0.042 \pm 0.007)\ \text{Å},$$
$$\delta \mathrm{Se}^{\mathrm{Exp}} = (0.014 \pm 0.004)\ \text{Å} \qquad (10)$$

for the displacements of the atoms in the single L_i component mode. These values correspond, for the complete $3L$ pattern, to the displacements

$$\overset{(3)}{\delta \mathrm{Ti}}{}^{\mathrm{Exp}} = (0.085 \pm 0.014)\ \text{Å},$$
$$\overset{(3)}{\delta \mathrm{Se}}{}^{\mathrm{Exp}} = (0.028 \pm 0.007)\ \text{Å} \qquad (11)$$

for the Ti and Se atoms that actually move (in a $3\boldsymbol{q}$ mode not all the atoms move). The experimental values for the displacements in a single $\boldsymbol{q}_{L_i}$ component mode are also shown on the diagram in Fig. 4 and correspond to the experimental estimate for the ratio

$$\nu^{\mathrm{Exp}} \equiv \delta \mathrm{Ti}^{\mathrm{Exp}}/\delta \mathrm{Se}^{\mathrm{Exp}} = 3.42 \pm 1.48. \qquad (12)$$

Motivated by these experimental results, we calculated the energy pattern of the $3\boldsymbol{q}_L$ mode in $\mathcal{V}_L^-$ for the studied cases. Moreover, in order to study the role played by the interaction between layers, we also calculated the energy pattern of the $3\boldsymbol{q}_M$ distortion in $\mathcal{V}_M^-$. The results are shown in Fig. 5. As we can see, a triple-$\boldsymbol{q}$ pattern returns always a structure more stable than the corresponding single-$\boldsymbol{q}$ displacement and it is always the $3\boldsymbol{q}_L$ distortion that gives the lowest energy (except, again, in the $\mathrm{GGA_{Th}}$ case where the modes $3\boldsymbol{q}_L$ and $3\boldsymbol{q}_M$ are almost degenerate). Moreover, as with the single-$\boldsymbol{q}$ patterns, if the cell dimensions are comparable, we find similar results, irrespective of the local functional used. For the GGA theoretical cell, which is larger than the experimental one, the system is more unstable as during the distortion the energy decrease is greater. In Table V, we report, for the minimum point of the $3\boldsymbol{q}_L$ energy pattern, the values of the energy variation (per supercell) and the shift of the atoms (for the component A_u single-$\boldsymbol{q}_L$ modes) with respect to the undistorted crystal. The values of the displacements for the studied cases, compared with the experimental result, are also shown in Fig. 6 (which corresponds to a portion of the diagram in Fig. 4). From the magnitude of the atomic displacements, we can see again that with the experimental cell the results

TABLE V. First column: largest energy gain (per supercell), with respect to the undistorted phase, for the $3\boldsymbol{q}_L$ triple pattern in $\mathcal{V}_L^-$. Second and third columns: corresponding atomic displacements, with respect to the undistorted phase, for the component single modes (A_u symmetry). Notice that for the resultant $3\boldsymbol{q}_L$ mode the displacement of the atoms that actually move is two times larger, cf. Fig. 3. First row: experimental measure of the displacement for the CDW phase with respect to the high-temperature phase [1].

	ΔE^{min} (meV)	δTi (Å)	δSe (Å)
EXP	–	0.042 ± 0.007	0.014 ± 0.004
$\mathrm{LDA_{Exp}}$	−8.4	0.030	0.010
$\mathrm{GGA_{Exp}}$	−7.4	0.027	0.011
$\mathrm{GGA_{Exp}^{VdW}}$	−6.8	0.026	0.010
$\mathrm{GGA_{Th}}$	−23.4	0.037	0.015
$\mathrm{GGA_{Th}^{VdW}}$	−8.3	0.028	0.011

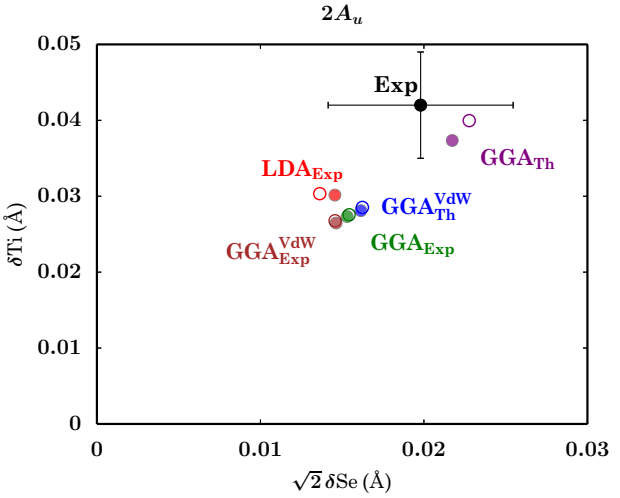

FIG. 6. (Color online) Filled points: displacement of the atoms corresponding to the energy minimum along the $3L$ pattern in $\mathcal{V}_L^-$ (single A_u component). Empty points: A_u component of the total displacement obtained by further relaxing the structure.

do not essentially depend on the local functional used. The results obtained in the $\mathrm{GGA_{Th}^{VdW}}$ case are also similar, the unit cell being similar to the experimental cell, whereas the displacement is greater in the $\mathrm{GGA_{Th}}$ case, which has a larger unit cell.

The fact that a $3\boldsymbol{q}_L$ pattern gives a structure more stable than the single $\boldsymbol{q}_L$ pattern is in agreement with the experimental findings but, in order to demonstrate that the *ab initio* calculations are able to predict the experimental results, it is necessary to go further and demonstrate that the $3\boldsymbol{q}_L$ pattern gives the most stable structure among all the possible distortions in $\mathcal{V}_L^-$. Since we expected analogous results in all the analyzed cases we just considered the $\mathrm{GGA_{Th}^{VdW}}$ one. In order to accomplish the task, we should have considered a uniform sample of the unit sphere in $\mathcal{V}_L^-$ and computed the energy path for an increasing modulus of the distortion along each of that directions. Instead, in order to reduce the workload, we just computed the energy of the system for distortions $\boldsymbol{d}$ having a fixed modulus $\|\boldsymbol{d}\| = \mathcal{D}$, where $\mathcal{D} = 0.146$ Å is a length approximately in half position between the minimum along the $\boldsymbol{q}_{L_i}$ and the $3\boldsymbol{q}_L$ patterns (cf. Fig. 5). In this way, we only needed to scan the energy of the system for a uniform grid on the two-dimensional sphere in $\mathcal{V}_L^-$ with radius $\mathcal{D}$. We used the basis $\hat{\boldsymbol{d}}_{L_i}$ to parametrize the space $\mathcal{V}_L^-$ and the fact that, given a general vector $\boldsymbol{d} = \sum_{i=1}^{3} c_i \hat{\boldsymbol{d}}_{L_i}$, all the other vectors obtained from it by changing the sign of its components c_i give equivalent distortions. Therefore, we considered only one octant of the sphere of radius $\mathcal{D}$ to obtain a general scan of the surface:

$$\boldsymbol{d} = \sum_{i=1}^{3} c_i \hat{\boldsymbol{d}}_{L_i}, \quad \sum_{i=1}^{3} |c_i|^2 = \mathcal{D}, \quad c_i > 0. \qquad (13)$$

A heat-map plot of the results obtained is showed in Fig. 7: our calculations confirm that on this sphere the $3\boldsymbol{q}_L$ pattern (which has components $c_i = \mathcal{D}/\sqrt{3}$) returns, among all the possible patterns in $\mathcal{V}_L^-$, the most stable structure. We conclude that, in the frame of the electron-phonon interaction, by using

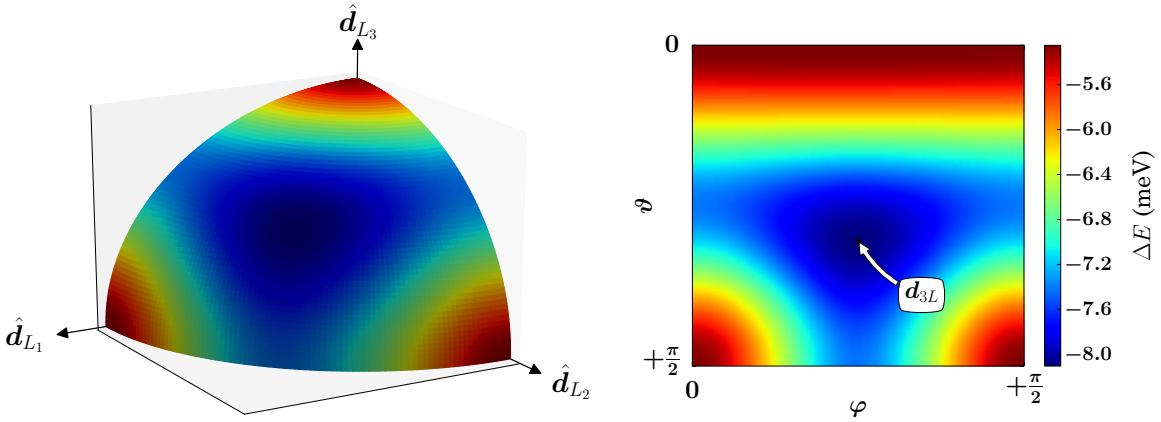

FIG. 7. (Color online) $\mathrm{GGA}_{\mathrm{Th}}^{\mathrm{VdW}}$ case: heat-map plot of the energy variation with respect to the undistorted phase for distortions corresponding to vectors in $\mathcal{V}_L^-$ having modulus $\mathcal{D} = 0.146$ Å. Due to the symmetry of the system, the result is shown on a single octant. (Left) 3D color plot on the spherical surface of radius $\mathcal{D}$. (Right) 2D plot in spherical coordinates (ϑ,φ) associated to the basis $(\hat{\boldsymbol{d}}_{L_i})$. The lowest energy is obtained for the $3\boldsymbol{q}_L$ distortion, whose angular coordinates are $\varphi = \pi/4$, $\vartheta = \arccos(1/\sqrt{3})$.

first-principles calculations, we are able to recover the CDW structural instability experimentally observed for $TiSe_2$.

E. Optimization of crystal structure in the CDW phase

In order to find the equilibrium configuration for the distorted system, we subsequently relaxed the structure starting from the configuration corresponding to the minimum of the energy along the $3\boldsymbol{q}_L$ path. We relaxed the whole structure (cell and internal positions) or only the internal positions depending on whether we were considering the theoretical or the (fixed) experimental cell. This led to a further small gain in energy with respect to the undistorted phase (see Table VI).

As it can be seen from Table VII, the effect of the relaxation on the lattice parameters is quite small, with a relative variation of the order of 10^{-3}. For the internal displacements, we define the vectors in $\mathcal{V}$, $\boldsymbol{d}^{\mathrm{min}}$ and $\boldsymbol{d}^{\mathrm{rlx}}$, characterizing the atomic shifts from the undistorted phase to the minimum along the $3\boldsymbol{q}_L$ path in $\mathcal{V}_L^-$ and the equilibrium position reached after the relaxation, respectively (in the theoretical cell cases $\boldsymbol{d}^{\mathrm{rlx}}$ is the relative displacement with respect to the cell). A quantitative measure of the extent of the additional atomic displacements due to the relaxation is obtained by comparing the modulus and the direction of these vectors. The results are shown in Table VII and, as we can see, the two vectors are very similar (only slightly different in the $\mathrm{GGA}_{\mathrm{Th}}$ case), meaning that the relaxation does not give an additional huge displacement of the atoms.

The total displacement $\boldsymbol{d}^{\mathrm{rlx}}$ is mainly made of a $3\boldsymbol{q}_L$ distortion but it also has a small component that changes the value of R shown in Fig. 1 (the value of this parameter being not fixed by the symmetry, anymore) and modifies the distances h_α and h_β between the non-equivalent Se(α) and Se(β) atoms and the Ti plane. As a consequence, in the distorted structure, the upper (and lower) Se atoms of a layer are not on the same plane anymore (cf. also Ref. [32]). The values found for the atomic displacements are reported in Table VI and, in particular, the updated values of δTi and δSe for the A_u component of the displacement are also shown in Fig. 6.

In order to test the reliability of our pseudopotentials and, consequently, of our conclusions, we also performed structural optimization by using the projector augmented wave (PAW) method [33]. We relaxed the internal structure of the undistorted and distorted phases obtained with LDA and GGA pseudopotentials with experimental cell by using corresponding projector augmented wave (PAW) potentials. We found that with PAW-LDA and PAW-GGA the instability is unaffected and the energies gained with distortion are in agreement with the ones obtained with LDA and GGA pseudopotentials, respectively, within an error of 1 meV. Therefore the incertitude due to the use of pseudopotentials is irrelevant in our problem.

TABLE VI. Effect of the relaxation on the minimum of the energy along the $3\boldsymbol{q}_L$ path in $\mathcal{V}_L^-$: the total variation of the energy (per supercell) from the undistorted phase ΔE^{rlx}, shifts δTi and δSe for the A_u component of the atomic displacements, variation of R (see Fig. 1), and change of h for the two non-equivalent atoms Se(α) and Se(β). First row: experimental measure of the displacement for the CDW phase with respect to the high-temperature phase [1].

	ΔE^{rlx} (meV)	δTi (Å)	δSe (Å)	$\delta R/R$	$\delta h_\alpha/h$	$\delta h_\beta/h$
EXP	–	0.042 ±0.007	0.014 ±0.004	–	–	–
$\mathrm{LDA}_{\mathrm{Exp}}$	−9.4	0.030	0.010	−0.0003	0.0011	−0.0001
$\mathrm{GGA}_{\mathrm{Exp}}$	−8.7	0.028	0.011	−0.0003	0.0016	0.0004
$\mathrm{GGA}_{\mathrm{Exp}}^{\mathrm{VdW}}$	−7.9	0.027	0.010	−0.0002	0.0014	0.0004
$\mathrm{GGA}_{\mathrm{Th}}$	−27.6	0.040	0.016	−0.0018	0.0031	−0.0038
$\mathrm{GGA}_{\mathrm{Th}}^{\mathrm{VdW}}$	−9.5	0.029	0.011	−0.0004	0.0010	−0.0006

TABLE VII. Effect of the relaxation on the minimum of the energy along the $3\boldsymbol{q}_L$ path in $\mathcal{V}_L^-$. First two rows: comparison of the vectors $\boldsymbol{d}^{\min}$ and $\boldsymbol{d}^{\mathrm{rlx}}$ representing the shifts of the internal atomic positions from the undistorted phase to the minimum of the energy along the $3\boldsymbol{q}_L$ path and the final relaxed configuration, respectively. Last two rows: relative variation of the cell parameters a and c (in the theoretical cell cases).

	$\frac{\|\boldsymbol{d}^{\mathrm{rlx}}\|}{\|\boldsymbol{d}^{\min}\|}$	$\frac{\langle \boldsymbol{d}^{\mathrm{rlx}} \mid \boldsymbol{d}^{\min}\rangle}{\|\boldsymbol{d}^{\mathrm{rlx}}\|\|\boldsymbol{d}^{\min}\|}$	$\frac{\Delta a}{a}$	$\frac{\Delta c}{c}$
$\mathrm{LDA_{Exp}}$	1.0008	0.9992	–	–
$\mathrm{GGA_{Exp}}$	1.0016	0.9981	–	–
$\mathrm{GGA_{Exp}^{VdW}}$	1.0022	0.9985	–	–
$\mathrm{GGA_{Th}}$	1.0392	0.9918	0.0006	0.0013
$\mathrm{GGA_{Th}^{VdW}}$	1.0046	0.9990	0.0006	0.0006

In conclusion, in this section, we have shown the results of a DFT pseudopotential structural analysis for $TiSe_2$ performed with several local functionals and experimental or theoretical lattice parameters. The results depend on the cell used and, in turn, the theoretical cell parameters depend on the local functional considered.

If the experimental cell is used, the results do not depend on the local functional used, the system becoming unstable in L (and M) with a A_u displacement pattern. Moreover, the distortion giving the most stable structure is the triple-point pattern in L, in agreement with neutron diffraction experiments for the CDW transition, and the magnitude of the distortion is not far from the experiment, the atomic displacements being slightly underestimated (especially for the Ti).

If we consider the LDA theoretical cell, which has lattice parameters smaller than the experimental ones, no instability is found. If we consider the GGA theoretical cell, which has the lattice parameter c quite larger than the experimental one, the instability is found but with atomic displacements and energy decrease greater than the ones obtained with the experimental cell. Finally, if we consider the GGA-type functional Grimme B97-D in order to describe better the Van der Waals forces, we obtain theoretical cell parameters quite similar to the experimental ones. Consistently, in this case, we obtain for the structural analysis results comparable to the ones obtained with the experimental cell. In Ref. [34], we provide the geometrical parameters for the distorted phase obtained in the studied cases.

IV. ELECTRONIC STRUCTURE IN THE CDW PHASE

A. Undistorted energy bands

In Fig. 8, we can see the undistorted bands of $TiSe_2$ around the Fermi level (E_F) for a high-symmetry path (cf. Refs. [18,32]). The atomic/orbital character of the bands is also

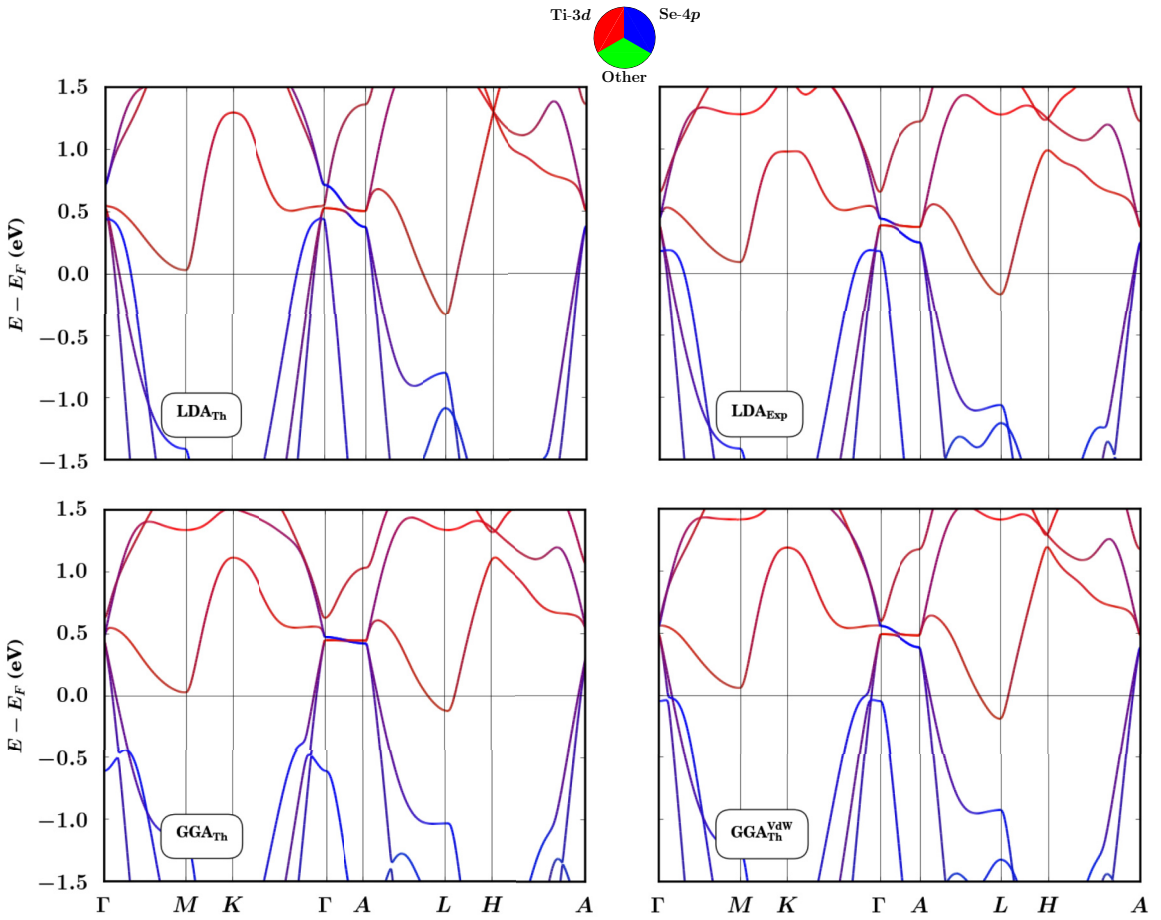

FIG. 8. (Color online) Band structure of $TiSe_2$ (undistorted phase) for several cases along a BZ high-symmetry line (cf. Fig. 2). The atomic/orbital character of bands is expressed by using different colors. The four cases shown have different unit cell parameters. Only in the $\mathrm{LDA_{Th}}$ case the system does not have a structural instability.

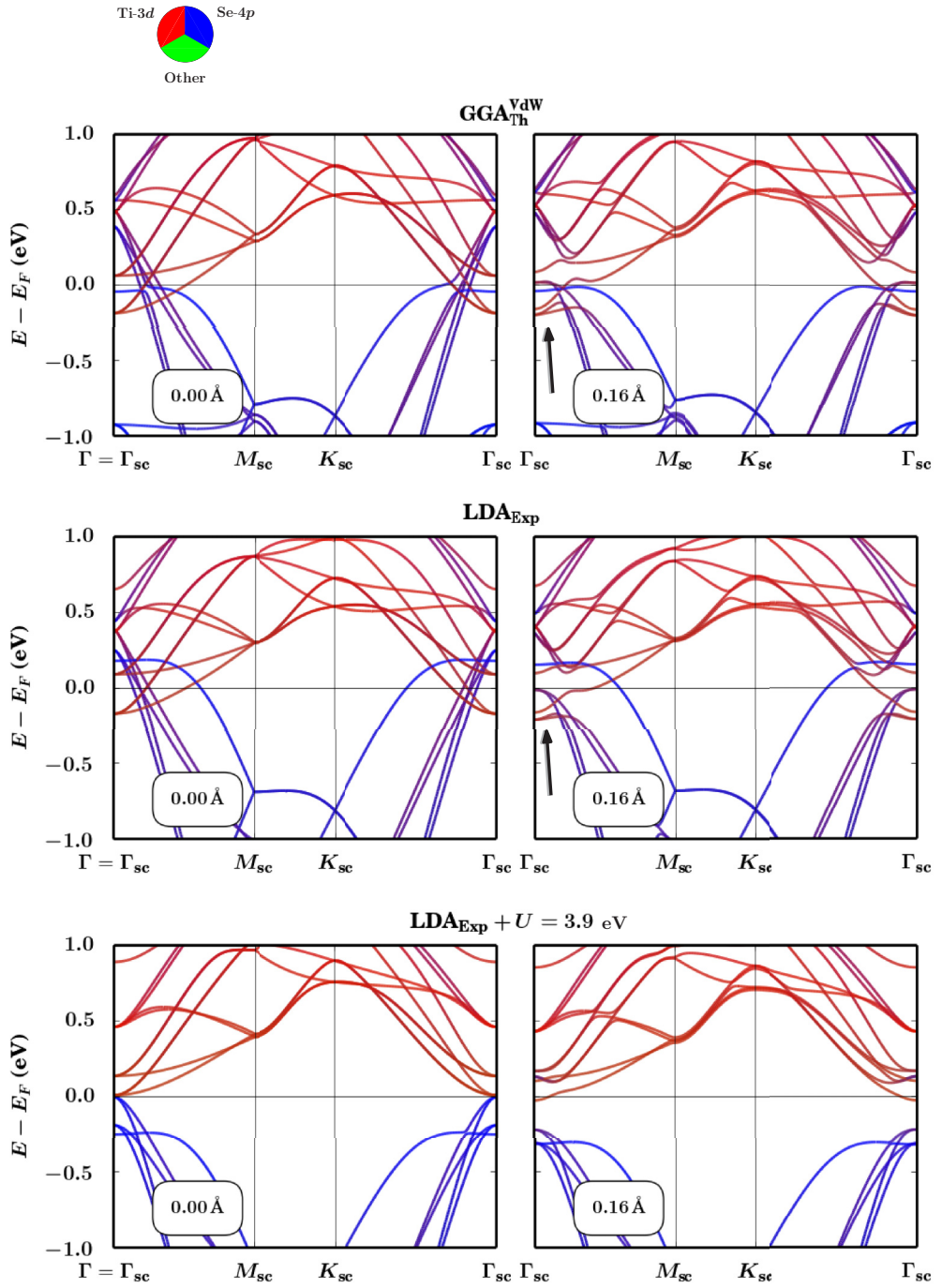

FIG. 9. (Color online) DFT bands, with orbital character, of the 2×2×2 superlattice along the high-symmetry line $\Gamma_{\rm sc}M_{\rm sc}K_{\rm sc}\Gamma_{\rm sc}$ of the supercell Brillouin zone. (Left) Undistorted configuration ($\|\boldsymbol{d}\| = 0.00$ Å). (Right) Distorted configuration ($\|\boldsymbol{d}\| = 0.16$ Å). An arrow highlights, in two cases, the effect of the repulsion between two Ti-3d bands.

shown (cf. Ref. [32]). In all the studied cases, we find similar results. Around the Fermi level there are only Ti-3d and Se-4p derived bands. In particular, a narrow Ti-3d band is almost entirely unoccupied except around the L point where it crosses the Fermi level and forms an electron pocket. Moreover, two Se-4p and Ti-3d strongly hybridized bands cross the Fermi level. Thus, in all these cases, the system appears to be metallic with a negative indirect band gap. However, a qualitative difference is found for a narrow Se-4p band whose position mostly depends on the cell parameters used but not on the local functional (calculations with the same unit cell but different local functionals give similar results). As a consequence, the shape of the calculated Fermi surface is very sensitive to the cell parameters used. Nevertheless, as we will see, this Se-4p band does not change during the CDW distortion.

B. Energy bands and DOS in the CDW phase

In this section, we discuss the evolution of the DFT band structure under the lowest energy 2×2×2 distortion found in $\mathcal{V}_L^-$. From now on we consider the cases LDA$_{\rm Exp}$ and GGA$_{\rm Th}^{\rm VdW}$.

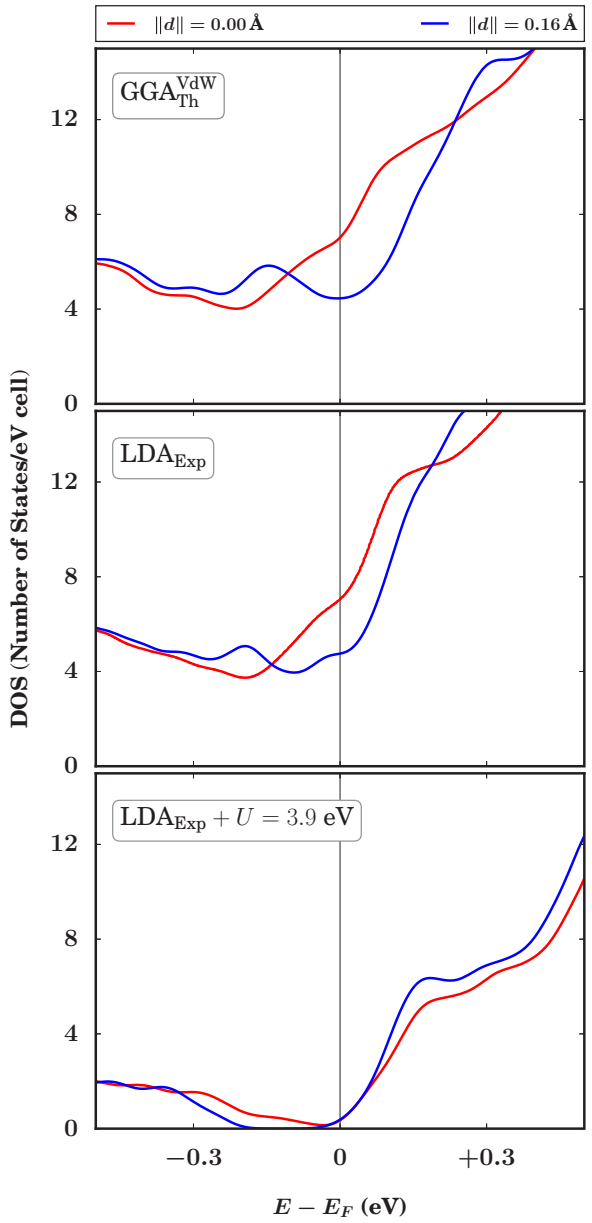

FIG. 10. (Color online) Density of states around the Fermi level for three cases in the undistorted (red line) and distorted (blue line) phases.

With the subscript "sc" below the labels Γ, M, K of the special points in the BZ, we refer to the corresponding points of the 2×2×2 supercell Brillouin zone (SBZ), which has the same shape of the BZ but half size.

In Fig. 9, we show the 2×2×2 bands, around the Fermi level, for a high-symmetry line of the SBZ for the undistorted and distorted phases, the last one corresponding to the minimum of the energy along the $3\boldsymbol{q}_L$ distortion path in $\mathcal{V}_L^-$. On formation of the superstructure, we observe a net change near the Fermi level with similar characteristics in the two cases. In particular, around $\Gamma_{\mathbf{sc}}$, we find avoided crossings at the Fermi level and, just below it, the appearance of a characteristic structure due to the repulsion of bands having Ti-3d character (see Fig. 9). As we will see in Sec. V A, this structure seems to describe a feature observed in the experiment. The Se-4p bands crossing the Fermi level around the wave vector $(1/2)\Gamma_{\mathbf{sc}}M_{\mathbf{sc}}$, instead, do not suffer any modification during the distortion, as anticipated. As expected, the change of the electronic dispersion around the Fermi level leads to a change of the density of states (DOS) as it is shown in Fig. 10. On forming the superlattice structure the DOS decreases by around 40% at E_F and a peak, essentially due to the Ti-3d orbitals, develops at 0.15/0.2 eV below E_F. These effects have been qualitatively observed in some previous theoretical works (see Ref. [16], for example, for a tight-binding study) and could be, at some level, compatible with the change of the resistivity experimentally observed in the CDW transition [1].

C. Energy band folding and unfolding

The superlattice distortion doubles the original lattice periodicity of the system. In fact, each eigenfunction $\Psi_{\boldsymbol{K},J}$ of the distorted system has the pseudomomentum $\boldsymbol{K}$ in the SBZ, which is one-eighth of the original BZ. Nevertheless, the function $\Psi_{\boldsymbol{K},J}$ is made of eight contributions $\psi^{\boldsymbol{K},J}_{\boldsymbol{k}_i}$ which are functions pseudoperiodic on the original lattice and whose pseudomomenta $\boldsymbol{k}_i$ are obtained by unfolding $\boldsymbol{K}$ into the original BZ:

$$\Psi_{\boldsymbol{K},J} = \sum_{i=1}^{8} \psi^{\boldsymbol{K},J}_{\boldsymbol{k}_i}. \tag{14}$$

The spectral weights $\omega^{\boldsymbol{K},J}_{\boldsymbol{k}_i}$:

$$\omega^{\boldsymbol{K},J}_{\boldsymbol{k}_i} \equiv \left\| \psi^{\boldsymbol{K},J}_{\boldsymbol{k}_i} \right\|^2, \quad \sum_{i=1}^{8} \omega^{\boldsymbol{K},J}_{\boldsymbol{k}_i} = 1, \tag{15}$$

can be used to evaluate the contributions to $\Psi_{\boldsymbol{K},J}$ coming from different points of the original BZ (see Appendix).

From geometrical considerations, we see that in our case the SBZ can be unfolded into eight regions of the BZ centered around the points Γ, A, L_i, M_i, respectively, and we can use this property to label the corresponding unfolding weights. Moreover, due to the threefold symmetry of the system, for a point $\boldsymbol{K}$, it is convenient to sum the contributions coming from the three equivalent L_i points, and the same for the contributions coming from the three M_i points: in this way, we have four contributions of type Γ, L, M, A depending on the BZ portion they came from. In Fig. 11, the weights of these four contributions on the bands are shown by means of a color code. In this way, we easily recognize, for example, that the characteristic band configuration under E_F in $\Gamma_{\mathbf{sc}}$ due to the repulsion of Ti-3d bands has a pure L character.

A complementary method to describe the 2×2×2 distortion in the frame of the original translation symmetry (and best suited to make a direct comparison with ARPES experiments) is to unfold the superlattice band structure from SBZ into the original BZ [35,36]. This consists in plotting, for the points $\boldsymbol{k}$ of a line in the BZ, the energy bands $E_{\boldsymbol{K},J}$ of the distorted system with an intensity $I^{\boldsymbol{K},J}_{\boldsymbol{k}}$ equal to the spectral weights $\omega^{\boldsymbol{K},J}_{\boldsymbol{k}}$ (for $I^{\boldsymbol{K},J}_{\boldsymbol{k}} = 0$, we have full transparency, i.e., no band, and for $I^{\boldsymbol{K},J}_{\boldsymbol{k}} = 1$ full opacity). In this way, the displacement of the atoms is observed as a distortion, smearing and fade of the original bands plus the appearance of new ghost bands.

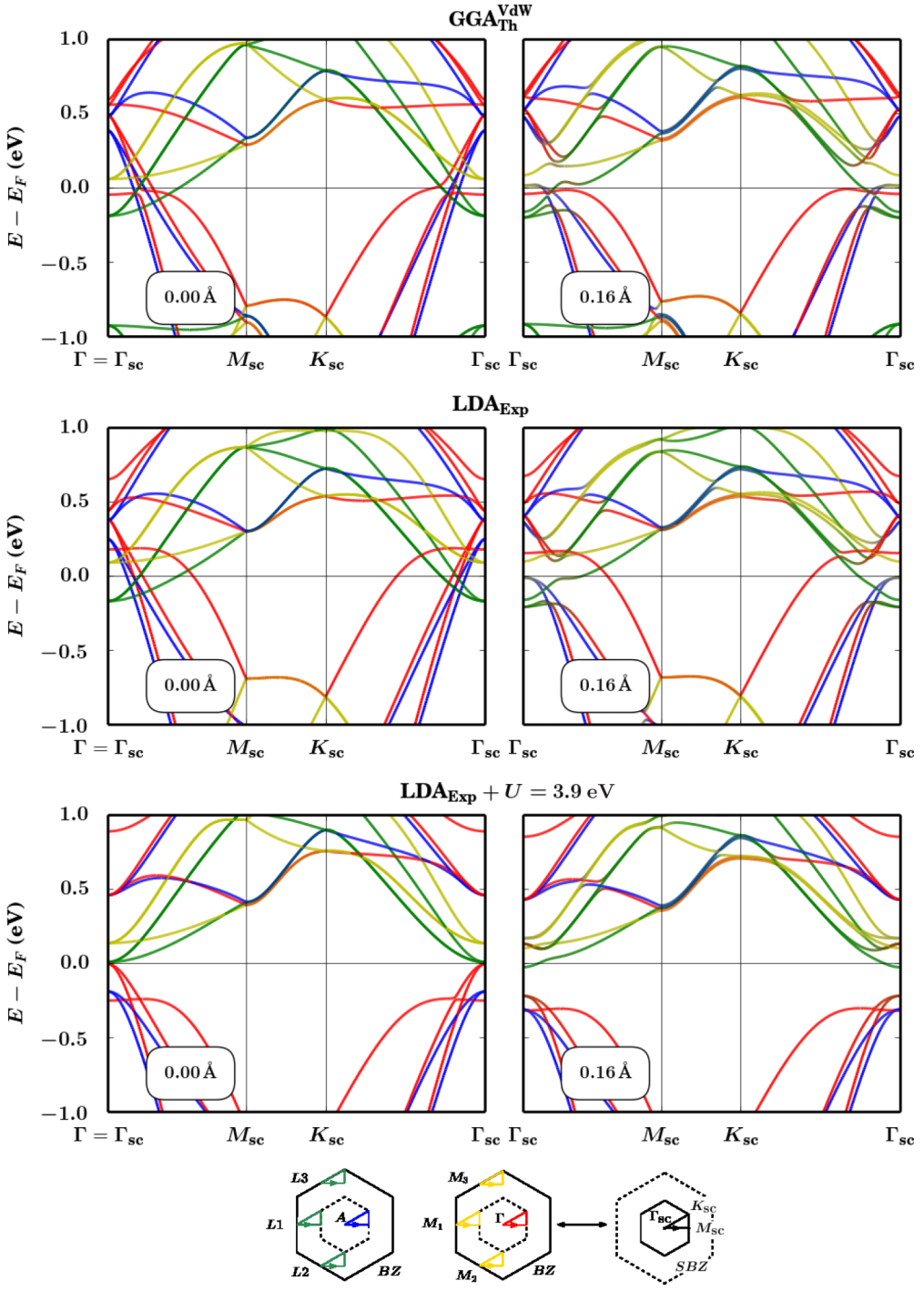

FIG. 11. (Color online) DFT bands of the 2×2×2 superlattice along the high-symmetry line $\Gamma_{sc}M_{sc}K_{sc}\Gamma_{sc}$ of the supercell Brillouin zone. (Left) Undistorted configuration ($\|\boldsymbol{d}\| = 0.00$ Å). (Right) Distorted configuration ($\|\boldsymbol{d}\| = 0.16$ Å). The colors indicate the weights of the corresponding eigenfunctions on different parts of the 1×1×1 Brillouin zone.

In Fig. 12, the unfolded bands with the orbital character are shown. In order to ease the comparison with the undistorted phase, we also superimpose the unfolded bands on the original band structure. From these figures, we can clearly see what is the principal effect of the 3L distortion: some of the bands with (partial) Ti-3d character do not cross the Fermi level anymore, whereas the Se-4p bands essentially remain unaffected, the net effect being the depletion around E_F seen in Fig. 10. Moreover, we see the appearance of a ghost band in L, which gives the characteristic structure we have already discussed.

V. COMPARISON WITH ARPES

A. LDA$_{Exp}$ and GGA$^{VdW}_{Th}$

In the previous sections, we analyzed the kind of distortion that lowers the total energy of the system and the consequent

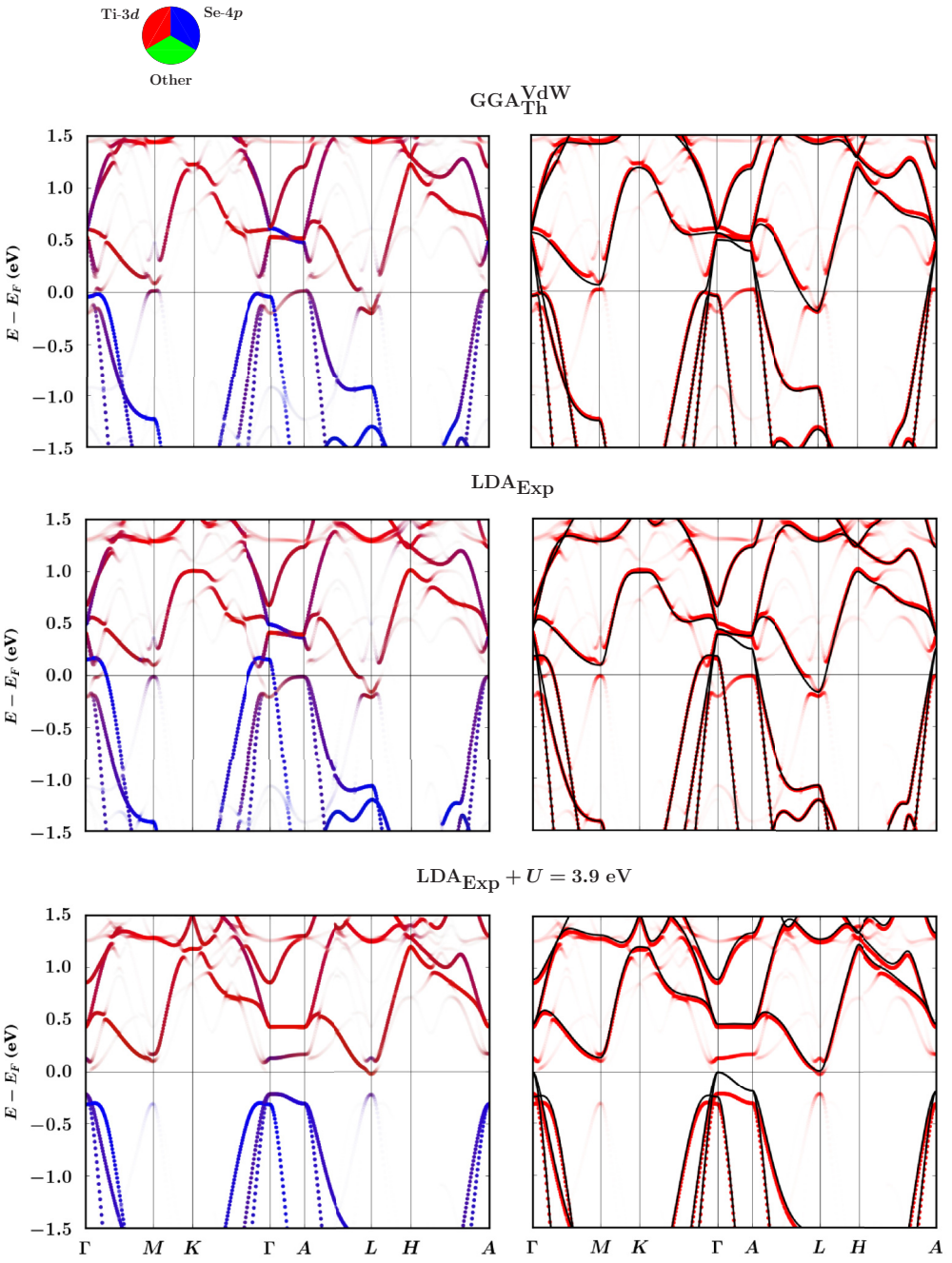

FIG. 12. (Color online) Unfolded bands for three cases. (Left) Unfolded bands for the distorted phase on a high-symmetry line of the original Brillouin zone with the orbital characters highlighted by colors. (Right) Unfolded bands (in red) superimposed on the undistorted bands (in black) along the same line.

changes in the electronic structure as they are found by *ab initio* DFT calculations. In this section, we compare the results of the calculated band structure with recent ARPES data taken from Ref. [37]. In Fig. 13, we show the DFT bands for the undistorted and distorted phases superimposed on the ARPES data taken at high ($T = 300$ K) and low ($T = 35$ K) temperature, respectively.

In $TiSe_2$, the electronic structure seems to depend crucially on $\boldsymbol{k}_z$ [10,38]. This is, for example, also demonstrated by the fact that standard pseudopotential DFT bands have an electron pocket in L but not in M. However, $\boldsymbol{k}_z$ is not a good quantum number in ARPES and so, given the nontrivial electronic structure of $TiSe_2$, there is not a clear $\boldsymbol{k}_z$ attribution in the experiments as a function of the incident energy. For these reasons (the indetermination of $\boldsymbol{k}_z$ in the ARPES and the substantial $\boldsymbol{k}_z$ dispersion in the electronic structure of $TiSe_2$), we consider the DFT bands along the two directions Γ-M and A-L in BZ. In the high-temperature case, we simply plot the bands along these two lines for the undistorted system, and in the low-temperature case, we plot the $2\times2\times2$ bands of the distorted structure unfolded into BZ along these two directions. In this second case, in order to ease the comparison

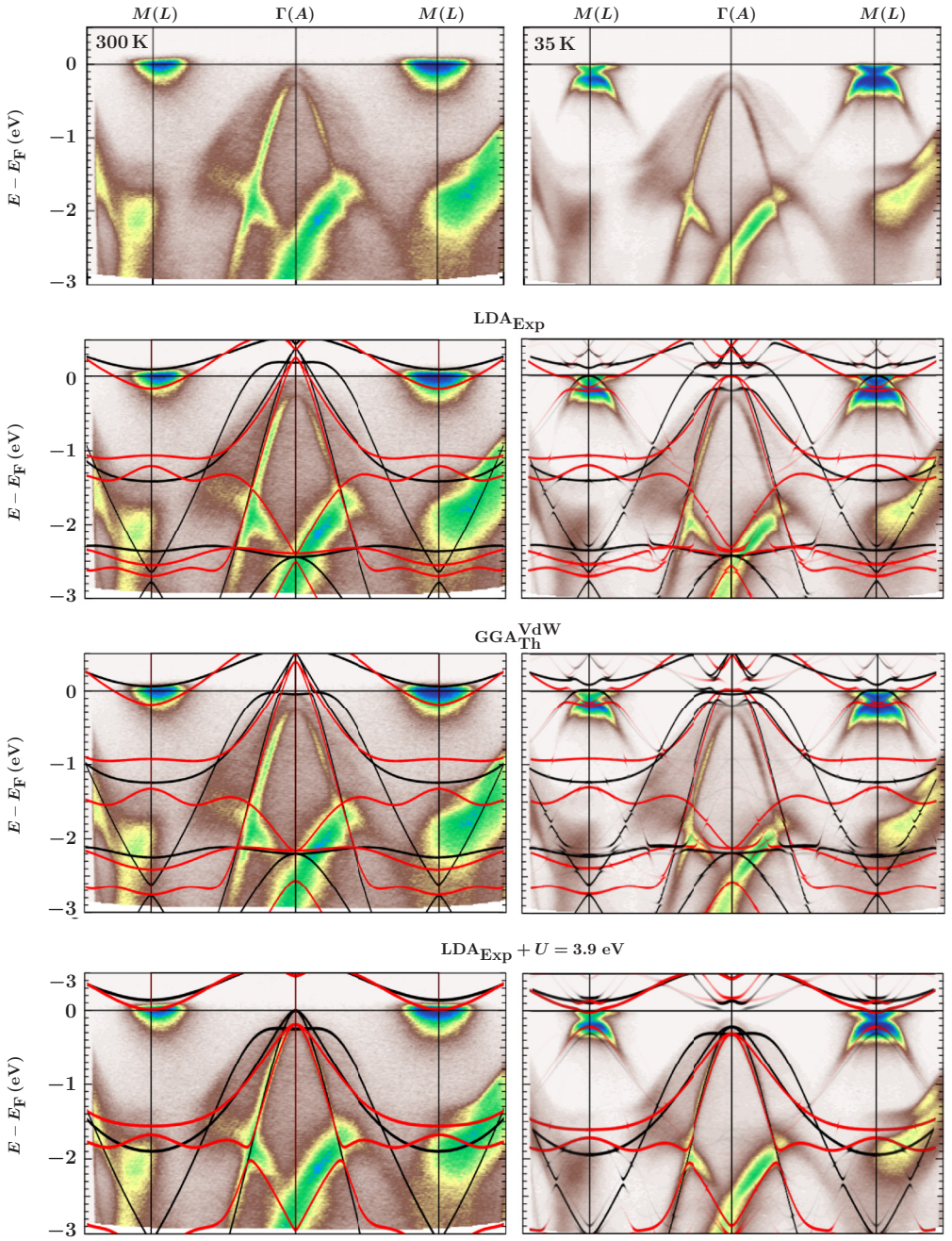

FIG. 13. (Color online) Comparison with ARPES data (from Ref. [37]) in three cases. First row: ARPES data taken at high temperature (left-hand panel, $T = 300$ K) and low temperature (right-hand panel, $T = 35$ K). Last three rows: DFT bands superimposed on the ARPES data. Black lines: Γ-M direction in BZ. Red lines: A-L direction in BZ. In the high-temperature cases, the bands of the undistorted structure are plotted. In the low-temperature cases, the $2\times2\times2$ bands of the distorted structure unfolded into the original BZ are plotted. The intensity of the unfolded ghost bands have been slightly enhanced in order to ease the comparison with the ARPES figure (see main text).

with the underlying figure, we slightly enhanced the intensity of the unfolded bands by scaling the whole transparency by a factor $f = 4$:

$$I_{\mathbf{k}}^{K,J} = f \cdot \omega_{\mathbf{k}}^{K,J}. \tag{16}$$

As anticipated, the structure in the distorted theoretical bands arising from the repulsion of the Ti-3d bands seems to reproduce a feature experimentally observed with ARPES in $M(L)$. Nevertheless, the overall agreement between the theoretical bands and ARPES data, both in the low- and high-temperature phases, is not good. Particularly, the large band overlap between the conduction and valence bands found in the undistorted phase is not compatible with the ARPES data considered.

It is worthwhile to recall that, in general, ARPES measures only occupied states, so the detection of states too close to

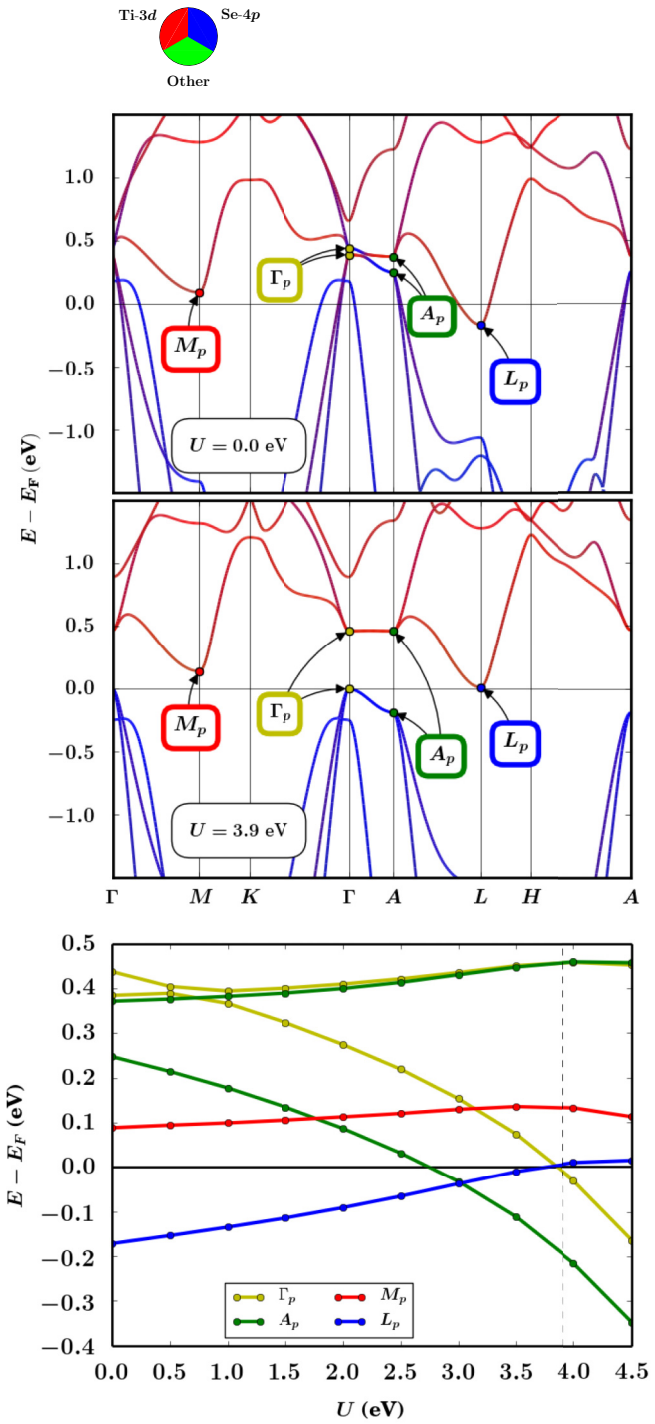

FIG. 14. (Color online) Effect of U on the bands. In the last figure, the vertical dashed line indicates the final self-consistent value $U \simeq 3.9$ eV, which corresponds to an insulating phase with a small gap of approximatively 0.014 eV.

the Fermi level can be very difficult. In literature, there are several works that have tried to estimate the energy dispersion around the Fermi level, especially the overlap/gap between the Se-4p valence band in Γ and the Ti-3d conduction band in L, sometimes with discordant results. Among the early works on the high-temperature phase, we can cite the paper by Anderson *et al.* [38], reporting an overlap (<120 meV) between these bands, and the paper by Traum *et al.* [39], which also estimates a degeneracy between the conduction and valence bands within 0.2 eV. In Ref. [40], Stoffel *et al.* claim a semiconductor band character in both high- and low-temperature phases with a bang gap of 0.06 eV and 0.02 eV, respectively, but leaving open the possibility of a slight overlap in the high-temperature phase due to the error uncertainty.

Among more recent works, Pillo *et al.* [41] estimate a small overlap between the conduction and valence band of ∼5 meV in the high-temperature phase, and a small positive gap in the low-temperature phase (however, with a semimetallic character in both the phases). Rossnagel *et al.* [10], instead, estimate a positive Se-4p/Ti-3d band gap increasing from 35 to 110 meV upon cooling from room temperature to 100 K (with an error bar of order of 30 meV). In Ref. [42], Kidd *et al.* describe a CDW transition from a very small gap semiconductor (∼0.05 eV) to another semiconductor with a larger gap (∼0.15 eV). In Ref. [43] Rasch *et al.*, by using H_2O surface absorption, identify $TiSe_2$ at room temperature as a semiconductor with a small gap of 150 ± 20 meV, whereas Li *et al.* [44] combine ARPES data with optical measurements and estimate a CDW transition between two semimetallic phases, with an overlap between the Se-4p and Ti-3d bands in the high-temperature phase compatible with the results in Ref. [18], and an open gap between the conduction and valence bands of ∼0.15 eV in the low-temperature phase.

Independently from the specific results or interpretations, the majority of modern works seems to converge toward similar conclusions. At high temperature, the positive or negative (i.e., overlap) indirect gap between Se-4p and Ti-3d bands is larger than the negative gap obtained with standard pseudopotential DFT calculations. Upon cooling the system, the CDW transition induces a distortion that either (slightly) increases the existing gap or leads to a gap opening between these bands, the value of the gap for the low-temperature phase being roughly around 0.1–0.15 eV. These results are also compatible with the ARPES data that we have considered in our comparisons.

A possible explanation for the mismatch found between theoretical bands and experiments could be the electron correlation effects due to the localized d orbitals of Ti, which are not properly taken into account in DFT-LDA or DFT-GGA calculations. We explored this possibility by using the LDA + U method and in the next section we show the results of this analysis.

B. $LDA_{Exp} + U$

As explained in Sec. II, we considered the Hubbard-like correction to the electronic structure of LDA_{Exp}. We used the experimental cell, the internal theoretical coordinates obtained with LDA and, on the top of this, the U correction for the Ti-3d orbitals. The most evident effect of introducing U is to open a gap between the bands with the result of obtaining, for $U \simeq 3.8$ eV, a metal-insulator transition (see Fig. 14). Motivated by this result, we found appropriate to estimate *ab initio* the proper value of U by using a self-consistent procedure. In a few steps, we obtained the converged value $U = 3.902$ eV for which the system is in an insulating phase with a small gap of approximatively 0.014 eV (see Fig. 14).

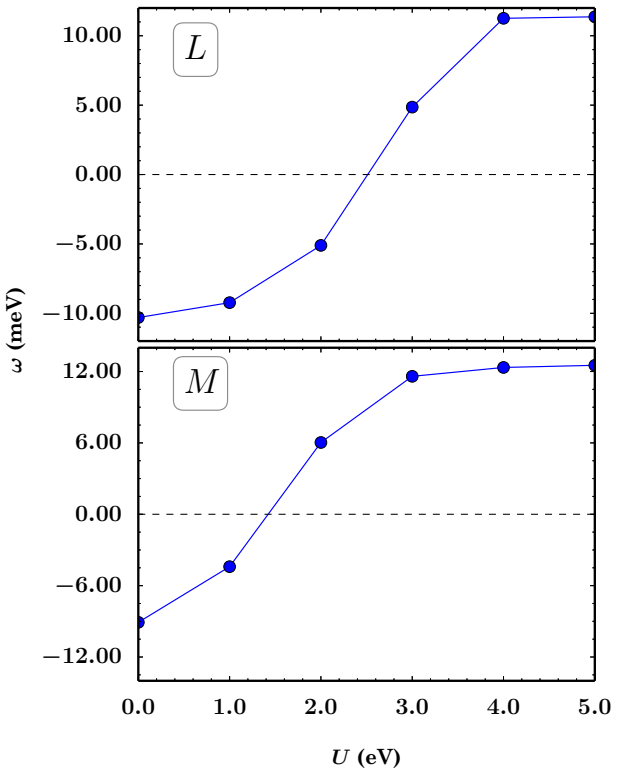

FIG. 15. (Color online) Lowest phonon frequency in L and M as a function of U, for the LDA + U system with the experimental cell and theoretical internal coordinates.

Therefore, the $\mathrm{LDA_{Exp}}$+U result seems to be closer to the experimental observations cited in the previous section than the large negative gap obtained with DFT calculations with standard local exchange-correlation functionals (cf. Sec. IV A, Fig. 8).

We used the same value of U also for the distorted structure found in the $\mathrm{LDA_{Exp}}$ case. We observed that the distortion has, on the electronic bands, the same qualitative effect already observed without U, the shift of the Ti-3d bands now increasing the initial small band gap up to a value of approximatively 0.2 eV (see Figs. 9–12). In the lowest panel of Fig. 13, we compare the calculated $\mathrm{LDA_{Exp}} + U$ bands with ARPES data: now the theoretical results for both the distorted and undistorted structures are in very good agreement with experimental data taken at high and low temperatures, respectively. However, as a result of a maybe slightly excessive gap opening, the structure that was observable for the distorted phase in the $\mathrm{LDA_{Exp}}$ and $\mathrm{GGA_{Th}^{VdW}}$ cases, resulting from the repulsion of the last two Ti-3d valence bands in L, now disappears (cf. Figs. 9 and 12).

According to these results, the correction provided by U seems to solve the dubious result regarding the comparison between the DFT electronic structure and the experiment, in particular by giving a good agreement between the theoretical bands and the ARPES data. Unfortunately, a serious drawback of this approach is that the presence of U eliminates the instability.

In Fig. 15, we show the lowest phonon frequency ω_L (ω_M) in L (M) as a function of U calculated by using the finite-difference method. When a phonon frequency ω is imaginary we conventionally indicate it with the negative value $-|\omega|$. We considered the LDA system with the experimental cell and internal coordinates now obtained by relaxing the atomic positions for each value of U. It can be observed that the frequencies, which are negative (i.e., imaginary) for $U = 0$ eV, increase as we increase U and begin to have a positive value around $U \simeq 2.5$ eV for ω_L and $U \simeq 1.5$ eV for ω_M. A phonon-converged calculation with this method was revealed to be extremely costly, especially for values of U close to the metal-insulator transition, therefore we also explicitly verified that the total energy of the system increases as we move the atoms along the expected distortion pattern. We performed similar tests also for the other functionals and we reached the same conclusion: the U corrected system is not unstable anymore for the value of U that seems to return the best agreement between the undistorted bands and the high-temperature ARPES data (notice that this value is functional-dependent, U being not a physical measurable quantity).

At this point, an intriguing question arises: on one hand, it seems that we are able to correct the energy band structure by using U, but on the other hand, the same correction spoils the prediction of the instability driven by the electron-phonon coupling, a prediction whose reliability, in turn, strongly depends on the correctness of the energy evaluation.

A possible explanation for this apparent paradox could be in the simplistic approach used to describe the structural instability with U. In general, the energy of a U corrected system (with cell fixed) is given by a function $\mathscr{E}(\boldsymbol{R}_i, U_j)$ of the atomic positions $\boldsymbol{R}_i$ and the values U_j for the orbitals. Moreover, for a certain atomic configuration $\boldsymbol{R}_i$, we have a proper value $U_j = \mathscr{U}_j(\boldsymbol{R}_i)$ for the Hubbard terms. So the total energy of the system as a function of the atomic positions, $E(\boldsymbol{R}_i)$, is given by

$$E(\boldsymbol{R}_i) = \mathscr{E}(\boldsymbol{R}_i, \mathscr{U}_j(\boldsymbol{R}_i)), \tag{17}$$

and when we consider the forces and the force constant matrix (through the first and second derivative of E with respect to the positions $\boldsymbol{R}_i$, respectively) we should take into account the full dependence on the atomic positions [28,45]. On the contrary, a commonly accepted procedure is to neglect the dependence of the Hubbard terms on $\boldsymbol{R}_i$ and to move the atoms by keeping fixed the values of U_j found for the undistorted system. This is the approach we considered in our study but its correctness seems to be questionable in this case since even a small variation of U (so small that it does not affect the energy bands position) leads to a total energy variation that is huge if compared with the energy decrease obtained with the distortion. For example, during the self-consistent calculation of U, we found that for $\Delta U \simeq 1$ meV the system has a variation of the total energy $\Delta E \simeq 8$ meV. In other words, we can suppose different values U_{und} and U_{dis} for the undistorted and distorted structures, respectively, with U_{dis} in principle (slightly) different from $U_{\mathrm{und}} \simeq 3.9$ eV (actually for the distorted phase we have two Ti atoms in non-equivalent positions, therefore we should properly consider two different parameters U_{dis}^1 and U_{dis}^2). For the distorted system, a very small variation of U_{dis} does not have any observable effect on the energy bands around the Fermi level, but it can give a total

energy higher (i.e., no instability) or lower (i.e., instability) than the undistorted one. This consideration has not to be confused with the results shown in Fig. 15 where, in order to restore the instability in L, a variation for U of at least 2.5 eV is required: in that calculation, the value of U for the Ti-3d orbital is kept fixed during the distortion.

Therefore, in general, we expect that in order to make a proper structural analysis of $TiSe_2$ with a U correction it is necessary to take into account the full position dependence (and consider that in the distorted phase we have two nonequivalent Ti sites with, in principle, two different values of U). However, it also means that, for example, a careful study of the convergence of U with the size of the supercell used to perform the perturbative calculation should be done. Nonetheless, it seems that, in general, the precision required for the value of U (at least 10^{-5} eV) is unrealistic and probably rules out the use of a U method in this form.

VI. CONCLUSIONS

In this work, we have presented a first-principles study of the charge-density wave in $TiSe_2$ by using DFT calculations with the harmonic approximation for the electron-phonon coupling. We have considered several local exchange-correlation functionals and both experimental and theoretical cell parameters.

As it is well known, in $TiSe_2$ the distance c between the layers is underestimated with LDA and overestimated with GGA. Thus, with these functionals it is impossible to have both the theoretical cell and pressure matching the experimental ones and a choice has to be made. A better result is obtained by using the semiempirical GGA-type functional Grimme B97-D, since it takes better into account the van der Waals forces acting between the layers of $TiSe_2$. With this functional, at zero theoretical pressure, the lattice parameters are quite in agreement with the experiment.

The results of the structural analysis strongly depend on the lattice parameters used. If the experimental unit cell is used, the system is unstable and similar results are obtained with different local functionals. On the contrary, with the LDA theoretical cell the system does not display any instability, whereas with the GGA theoretical cell the system displays an instability larger than the one obtained with the experimental cell (i.e., for the distorted phase, both the energy gain and the atomic displacements are greater with the theoretical cell than with the experimental cell). With Grimme B97-D the theoretical and experimental cells give analogous results.

The instabilities found in the calculations correspond to distortions in the L and M points of the BZ with symmetry A_u. In both cases, the most stable distortion is obtained by combining with equal weights the three rotational-symmetric degenerate patterns (the triple-point patterns in M and in L). The difference between the patterns in L and in M is only in the phase between two adjacent layers, the atomic displacements for adjacent layers being the same for the M patterns and the opposite for the L patterns. Since we have found an instability in both points, with the same kind of pattern, we can conclude that, as expected, the intralayer interactions are of paramount importance in order to give the structural instability of $TiSe_2$. Nonetheless, as long as the layers are close enough to have a significant interaction, the L distortions are always more favorable than the M ones, meaning that the interlayer interaction is not negligible in the CDW transition (with the GGA theoretical cell the corresponding energy patterns for L and M distortions are instead degenerate, the distance between layers being quite large in this case). Notice, however, that the interlayer interaction affecting the lattice instability is not of van der Waals type since, with the experimental cell, the calculations with the simple GGA or the GGA-type B97-D functional return analogous results. As a consequence, the van der Waals forces between the layers have to be taken into account in order to correctly estimate the distance between layers but they do not have effect on the energy of the lattice distortions. This, in some sense, legitimizes the choice of analyzing the CDW instability with the experimental cell, irrespective of the theoretical pressure (whose value depends on the functional used). Moreover, the dependence of the instability on the lattice parameters observed in calculations is compatible with the CDW suppression observed in experiments at high pressure.

The configuration with the lowest energy is a triple-$\boldsymbol{q}_L$ pattern, in agreement with the results of neutron diffraction experiments. The magnitude of the corresponding atomic distortion is not far from the experimental one. These results are in agreement with the tight-binding results in Ref. [3]. However, in those calculations, no phonon softening is found in M. This is an important difference with respect to our results.

We have also analyzed the electronic structure of the system. In the undistorted phase, the standard calculations (LDA and GGA-type functionals) give a metallic system with quite a large negative indirect gap. In this case, the choice of the lattice parameters is important too: the position of a Se-4p band crossing the Fermi level, and so the Fermi surface, is affected by the values of the unit cell parameters (but with fixed experimental cell parameters it is independent of the local functional used). In the experiment, the phase transition is accompanied by changes in the transport properties. With the distortion we observe modifications in the calculated bands near the Fermi level and a resulting depletion in the DOS (this result is compatible with the theoretical results in Ref. [3]).

We have compared the theoretical bands of the undistorted and distorted phases with the results of an ARPES experiment at high and low temperatures, respectively. For the distorted phase, the bands of the superstructure have been unfolded into the undistorted BZ in order to ease the comparison. Due to the distortion, the energy bands undergo a deformation that seems to reproduce some effects observed in ARPES. Nonetheless, the bands for both the undistorted and distorted phases are not in good agreement with ARPES data.

In order to correct the mismatch between ARPES data and band calculations, we have explored the role of the correlation for the Ti-3d electrons by performing an LDA + U calculation with the experimental cell. We have estimated *ab initio*, self-consistently, the value of the parameter U for the localized Ti-3d orbital in the LDA_{Exp} undistorted structure. For this value of U, the Hubbard-like correction opens a small indirect gap in the electronic bands of the undistorted phase. This result seems to be closer to the experimental observations than the ones

obtained with standard local exchange-correlation functionals. More importantly, the LDA + U bands are in good agreement with the results of a high-temperature ARPES experiment. By using the same value of U for the distorted structure, we have seen that the CDW increases the size of the undistorted phase band gap. The unfolded bands of the distorted phase are in good agreement with the low-temperature ARPES data too.

The drawback of the LDA + U approach is that the U correction removes the instability, the phonon frequency in M and L becoming real as we increase the value of U. A possible explanation for this effect is that the total energy in $TiSe_2$ depends very much on U. Therefore, the energy scale of our interest requires a very high precision on the value of U, which is out of the ordinary use and, probably, not even achievable. In particular, an accurate evaluation of U should also take into account the usually neglected, but in principle existing, dependence of U on the atomic positions.

In conclusion, we have shown that the CDW structural instability in $TiSe_2$ can be predicted with DFT local exchange-correlation functional calculations if the experimental unit cell is used, irrespective of the local functional adopted. Analogous results are obtained for the structural analysis if the Grimme B97-D functional with theoretical cell is used, in this case, the theoretical cell being in good agrement with the experimental one. As a consequence, with the Grimme B97-D functional the structural instability can be considered fully *ab initio* predicted.

In principle, DFT is an exact many-body theory so with the exact exchange-correlation functional it would be able to recover all the possible correlation effects. Nevertheless, since in practice we use different local functionals, which are obviously only approximatively correct, the robustness of our results at fixed experimental cell should be considered a proof that in the harmonic approximation it is possible to recover the CDW instability only by considering the lattice degree of freedom, i.e., the electron-phonon coupling, without considering any electron many-body effect. This confirms one of the results present in the experimental paper by Porer *et al.* in Ref. [11], namely that the CDW survives even if the electronic ordering is quenched.

On the other hand, calculations of the electronic structure show that DFT with ordinary local exchange-correlation functionals is not able to fully account for all the experimental findings, especially the ARPES measurements. The simple correction provided by the Hubbard-like U term improves this aspect considerably, but it doest not provide a full satisfactory picture as it spoils the phonon instability. As argued, this is only an apparent contradiction since it is probably related to an intrinsic weakness of the simplistic U correction adopted. Nonetheless, it appears necessary to consider a higher level exchange-correlation functional in order to give a full complete description of $TiSe_2$ through DFT calculations. Of course, since the displacement of the atoms influences the electron screening and, hence, the electron-phonon coupling, we expect that a better description of the electron exchange-correlation effects should also influence the distortion (i.e., the energy pattern and the magnitude of the atomic displacements), even if the CDW has a lattice origin. These represent open issues that deserve to be examined in future studies.

ACKNOWLEDGMENTS

The authors acknowledge financial support of the Graphene Flagship and of the Agence Nationale de la Recherche funds within the *Investissements d'Avenir* program under reference ANR-13-IS10-0003-01. Computer facilities were provided by CINES, CCRT, IDRIS, and by the project Equip@Meso (reference ANR-10-EQPX-29-01). The authors are grateful to K. Rossnagel, for having supplied to them the image data of ARPES experiment as well as detailed explanations of the measures realized, and to M. Cococcioni for useful discussions about the DFT+U method. R. Bianco thanks L. Paulatto for the support given in the use of QUANTUM ESPRESSO package.

APPENDIX: FOLDING AND UNFOLDING, DEFINITION OF THE SPECTRAL WEIGHTS

We label with $\mathscr{R}$ and $\widetilde{\mathscr{R}}$ the direct and reciprocal lattice vectors of the unit cell, respectively. Moreover, we define $\mathscr{R}_{\rm sc}$ and $\widetilde{\mathscr{R}}_{\rm sc}$ as the direct and reciprocal lattice vectors of the $2\times2\times2$ supercell, respectively. We find eight vectors $\boldsymbol{G}_i \in \widetilde{\mathscr{R}}_{\rm sc}$ (defined up to a vector of $\widetilde{\mathscr{R}}$) whose differences are not vectors of $\widetilde{\mathscr{R}}$:

$$\boldsymbol{G}_i \in \widetilde{\mathscr{R}}_{\rm sc}, \quad \boldsymbol{G}_i - \boldsymbol{G}_j \notin \widetilde{\mathscr{R}}. \tag{A1}$$

In the coordinates relative to $\widetilde{\mathscr{R}}$ it is, for example,

$$\begin{aligned} &\boldsymbol{G}_0 = (0.0,0.0,0.0), \quad \boldsymbol{G}_1 = (0.0,0.0,0.5),\\ &\boldsymbol{G}_2 = (0.5,0.0,0.0), \quad \boldsymbol{G}_3 = (0.5,0.0,0.5),\\ &\boldsymbol{G}_4 = (0.0,0.5,0.0), \quad \boldsymbol{G}_5 = (0.0,0.5,0.5),\\ &\boldsymbol{G}_6 = (0.5,0.5,0.0), \quad \boldsymbol{G}_7 = (0.5,0.5,0.5). \end{aligned} \tag{A2}$$

By using these vectors, we can unfold a general $\boldsymbol{K} \in$ SBZ into eight $\boldsymbol{k}_i \in$ BZ:

$$\boldsymbol{k}_i = \boldsymbol{K} + \boldsymbol{G}_i, \tag{A3}$$

and write

$$\Psi_{\boldsymbol{K},J} = \sum_{i=1}^{8} \mathcal{P}_{\boldsymbol{k}_i}(\Psi_{\boldsymbol{K},J}), \tag{A4}$$

where $\mathcal{P}_{\boldsymbol{k}_i}$ is the projector on the space of the Bloch functions having pseudomomentum $\boldsymbol{k}_i$ with respect to $\mathscr{R}$, that is, $\mathcal{P}_{\boldsymbol{k}_i}(\Psi_{\boldsymbol{K},J})$ is a function $\psi^{\boldsymbol{K},J}_{\boldsymbol{k}_i}(\boldsymbol{x})$ such that

$$\psi^{\boldsymbol{K},J}_{\boldsymbol{k}_i}(\boldsymbol{x}+\boldsymbol{r}) = e^{i\boldsymbol{k}_i\cdot\boldsymbol{r}}\,\psi^{\boldsymbol{K},J}_{\boldsymbol{k}_i}(\boldsymbol{x}), \quad \forall\,\boldsymbol{r} \in \mathscr{R}. \tag{A5}$$

The square modulus of $\mathcal{P}_{\boldsymbol{k}_i}(\Psi_{\boldsymbol{K},J})$ is, by definition, the unfolded weight $\omega^{\boldsymbol{K},J}_{\boldsymbol{k}_i}$ of the superlattice band $(\boldsymbol{K},J)$ in $\boldsymbol{k}_i$:

$$\omega^{\boldsymbol{K},J}_{\boldsymbol{k}_i} \equiv \left\|\mathcal{P}_{\boldsymbol{k}_i}(\Psi_{\boldsymbol{K}J})\right\|^2. \tag{A6}$$

In order to plot the unfolded energy spectrum along a high-symmetry line of BZ, we considered, for each $\boldsymbol{k}_0$ of this line, the superstructure eigenvectors $\Psi_{\boldsymbol{K}(\boldsymbol{k}_0),J}$ and eigenvalues $E_{\boldsymbol{K}(\boldsymbol{k}_0),J}$, $\boldsymbol{K}(\boldsymbol{k}_0)$ being the SBZ point into which $\boldsymbol{k}_0 \in$ BZ folds

$$\boldsymbol{K}(\boldsymbol{k}_0) = \boldsymbol{k}_0 - \boldsymbol{G}_0 = \boldsymbol{k}_0. \tag{A7}$$

Then we plotted the bands $E_{\boldsymbol{K}(\boldsymbol{k}_0),J}$ with intensity

$$I_{\boldsymbol{k}_0}^{\boldsymbol{K}(\boldsymbol{k}_0),J} = \omega_{\boldsymbol{k}_0}^{\boldsymbol{K}(\boldsymbol{k}_0),J}. \tag{A8}$$

$I_{\boldsymbol{k}_0}^{\boldsymbol{K}(\boldsymbol{k}_0),J} = 0$ corresponding to full transparency (no band) and $I_{\boldsymbol{k}_0}^{\boldsymbol{K}(\boldsymbol{k}_0),J} = 1$ to full opacity.

Notice that, properly speaking, $\boldsymbol{k}_0$ and $\boldsymbol{K}(\boldsymbol{k}_0)$ are not simple vectors: they represent classes of vectors defined up to the sum with an element in $\widetilde{\mathscr{R}}$ and $\widetilde{\mathscr{R}}_{\rm sc}$, respectively. Thus, even if the representatives $\boldsymbol{k}_0$ and $\boldsymbol{K}(\boldsymbol{k}_0)$ are equal, they refer to different sets of vectors.

[1] F. J. Di Salvo, D. E. Moncton, and J. V. Waszczak, Phys. Rev. B **14**, 4321 (1976).
[2] M. Holt, P. Zschack, H. Hong, M. Y. Chou, and T.-C. Chiang, Phys. Rev. Lett. **86**, 3799 (2001).
[3] K. Motizuki, *Structural Phase Transitions in Layered Transition Metal Compounds*, Physics and Chemistry of Materials with A (Springer, Netherlands, Dordrecht, 1986).
[4] S. Hellmann, T. Rohwer, M. Kallne, K. Hanff, C. Sohrt, A. Stange, A. Carr, M. Murnane, H. Kapteyn, L. Kipp, M. Bauer, and K. Rossnagel, Nat. Commun. **3**, 1069 (2012).
[5] K. Rossnagel, J. Phys.: Condens. Matter **23**, 213001 (2011).
[6] H. Cercellier, C. Monney, F. Clerc, C. Battaglia, L. Despont, M. G. Garnier, H. Beck, P. Aebi, L. Patthey, H. Berger, and L. Forró, Phys. Rev. Lett. **99**, 146403 (2007).
[7] J. A. Wilson, Phys. Status Solidi B **86**, 11 (1978).
[8] J. A. Wilson, Solid State Commun. **22**, 551 (1977).
[9] H. P. Hughes, J. Phys. C **10**, L319 (1977).
[10] K. Rossnagel, L. Kipp, and M. Skibowski, Phys. Rev. B **65**, 235101 (2002).
[11] M. Porer, U. Leierseder, J.-M. Ménard, H. Dachraoui, L. Mouchliadis, I. E. Perakis, U. Heinzmann, J. Demsar, K. Rossnagel, and R. Huber, Nat. Mater. **13**, 857 (2014).
[12] J. van Wezel, P. Nahai-Williamson, and S. S. Saxena, Phys. Rev. B **81**, 165109 (2010).
[13] E. Morosan, Zandbergen, B. S. Dennis, J. W. G. Bos, Y. Onose, T. Klimczuk, A. Ramirez, N. P. Ong, and R. J. Cava, Nat. Phys. **2**, 544 (2006).
[14] A. F. Kusmartseva, B. Sipos, H. Berger, L. Forró, and E. Tutiš, Phys. Rev. Lett. **103**, 236401 (2009).
[15] Y. Yoshida and K. Motizuki, J. Phys. Soc. Jpn. **49**, 898 (1980).
[16] N. Suzuki, A. Yamamoto, and K. Motizuki, J. Phys. Soc. Jpn. **54**, 4668 (1985).
[17] N. Suzuki, H. Yoshiyama, K. Motizuki, and Y. Takaoka, Synth. Met. **19**, 887 (1987)
[18] A. Zunger and A. J. Freeman, Phys. Rev. B **17**, 1839 (1978).
[19] M. Calandra and F. Mauri, Phys. Rev. Lett. **106**, 196406 (2011).
[20] S. Grimme, J. Comput. Chem. **27**, 1787 (2006).
[21] P. Giannozzi, S. Baroni, N. Bonini, M. Calandra, R. Car, C. Cavazzoni, D. Ceresoli, G. L. Chiarotti, M. Cococcioni, I. Dabo, A. Dal Corso, S. de Gironcoli, S. Fabris, G. Fratesi, R. Gebauer, U. Gerstmann, C. Gougoussis, A. Kokalj, M. Lazzeri, L. Martin-Samos, N. Marzari, F. Mauri, R. Mazzarello, S. Paolini, A. Pasquarello, L. Paulatto, C. Sbraccia, S. Scandolo, G. Sclauzero, A. P. Seitsonen, A. Smogunov, P. Umari, and R. M. Wentzcovitch, J. Phys.: Condens. Matter **21**, 395502 (2009).
[22] J. P. Perdew and A. Zunger, Phys. Rev. B **23**, 5048 (1981).
[23] J. P. Perdew, K. Burke, and M. Ernzerhof, Phys. Rev. Lett. **77**, 3865 (1996).
[24] S. Baroni, S. de Gironcoli, A. Dal Corso, and P. Giannozzi, Rev. Mod. Phys. **73**, 515 (2001).
[25] H. J. Monkhorst and J. D. Pack, Phys. Rev. B **13**, 5188 (1976).
[26] C. Riekel, J. Solid State Chem. **17**, 389 (1976).
[27] M. Cococcioni and S. de Gironcoli, Phys. Rev. B **71**, 035105 (2005).
[28] B. Himmetoglu, A. Floris, S. de Gironcoli, and M. Cococcioni, Int. J. Quantum Chem. **114**, 14 (2014).
[29] D. Alf, Comput. Phys. Commun. **180**, 2622 (2009).
[30] H. J. Kulik, M. Cococcioni, D. A. Scherlis, and N. Marzari, Phys. Rev. Lett. **97**, 103001 (2006).
[31] M. H. Whangbo and E. Canadell, J. Am. Chem. Soc. **114**, 9587 (1992).
[32] R. A. Jishi and H. M. Alyahyaei, Phys. Rev. B **78**, 144516 (2008).
[33] P. E. Blöchl, Phys. Rev. B **50**, 17953 (1994).
[34] See Supplemental Material at http://link.aps.org/supplemental/10.1103/PhysRevB.92.094107 for a database of the parameters for the distorted phase obtained in the studied cases. We provide the parameters obtained by minimizing the energy along the distortion path and by subsequently relaxing the structure.
[35] V. Popescu and A. Zunger, Phys. Rev. Lett. **104**, 236403 (2010).
[36] W. Ku, T. Berlijn, and C.-C. Lee, Phys. Rev. Lett. **104**, 216401 (2010).
[37] T. Rohwer, S. Hellmann, M. Wiesenmayer, C. Sohrt, A. Stange, B. Slomski, A. Carr, Y. Liu, L. M. Avila, M. Kallne, S. Mathias, L. Kipp, K. Rossnagel, and M. Bauer, Nature (London) **471**, 490 (2011).
[38] O. Anderson, R. Manzke, and M. Skibowski, Phys. Rev. Lett. **55**, 2188 (1985).
[39] M. M. Traum, G. Margaritondo, N. V. Smith, J. E. Rowe, and F. J. Di Salvo, Phys. Rev. B **17**, 1836 (1978).
[40] N. G. Stoffel, S. D. Kevan, and N. V. Smith, Phys. Rev. B **31**, 8049 (1985).
[41] T. Pillo, J. Hayoz, H. Berger, F. Lévy, L. Schlapbach, and P. Aebi, Phys. Rev. B **61**, 16213 (2000).
[42] T. E. Kidd, T. Miller, M. Y. Chou, and T.-C. Chiang, Phys. Rev. Lett. **88**, 226402 (2002).
[43] J. C. E. Rasch, T. Stemmler, B. Müller, L. Dudy, and R. Manzke, Phys. Rev. Lett. **101**, 237602 (2008).
[44] G. Li, W. Z. Hu, D. Qian, D. Hsieh, M. Z. Hasan, E. Morosan, R. J. Cava, and N. L. Wang, Phys. Rev. Lett. **99**, 027404 (2007).
[45] H. J. Kulik and N. Marzari, J. Chem. Phys. **135**, 194105 (2011).
[46] M. Calandra and F. Mauri, Phys. Rev. Lett. **112**, 049702 (2014).